SRNL-STI-2011-00006
Revision 1

Keywords: DWPF, SB7, Hg, ammonia, hydrogen

Retention: *Permanent*

Sludge Batch 7 Qualification and Flowsheet Chemical Process Cell Simulations

A.I. Fernandez
D.C. Koopman

May 12, 2011

Savannah River National Laboratory
Savannah River Nuclear Solutions
Aiken, SC 29808

Prepared for the U.S. Department of Energy under contract number DE-AC09-08SR22470.

SRNL
SAVANNAH RIVER NATIONAL LABORATORY

DISCLAIMER

Printed in the United States of America

Prepared for
U.S. Department of Energy

REVIEWS AND APPROVALS

AUTHORS:

D. C. Koopman, Process Technology Programs Date

TECHNICAL REVIEW:

M. E. Stone, Process Technology Programs Date

APPROVAL:

C. C. Herman, Manager Date
Process Technology Programs

S.L. Marra, Manager Date
Environmental & Chemical Process Technology Research Programs

J. E. Occhipinti, Manager Date
Waste Solidification Engineering

EXECUTIVE SUMMARY

The Defense Waste Processing Facility (DWPF) will transition from Sludge Batch 6 (SB6) processing to Sludge Batch 7 (SB7) in fiscal year 2011. SB7 consists of material from Tanks 4, 7, and 12. Tests were conducted using non-radioactive simulants of the expected SB7 compositions, both blend and qualification types, to determine the impact of varying the acid stoichiometry and oxalate concentration during the Sludge Receipt and Adjustment Tank (SRAT) and Slurry Mix Evaporator (SME) processes.

Four qualification runs and five flowsheet runs were performed to simulate the physical and chemical behavior of the Tank 51 material and the blended Tank 51/40 sludge, respectively. The simulants were called SB7-Q and SB7-A. These were produced in the SRNL Continuous Stirred Tank Reactor (CSTR).

The testing covered the domain from 100 to 150% of the Koopman minimum acid (KMA) equation or about 102 to 155% using the current DWPF-Hsu acid equation. The high acid runs produced the highest hydrogen gas generation but both the flowsheet and qualification cases never exceeded about 85% of the maximum allowable rate in the SRAT and SME cycles. The acid processing window for SB7 is approximately 102 to 155% according to the Hsu equation. It is recommended that 112% Hsu be used for SB7 processing.

Nitrite ion concentrations were reduced to 760 and <100 mg/kg slurry in the qualification and flowsheet 100% acid (KMA) SRAT products. These indicate that the Koopman equation accurately models the acid needs of SB7-Q and those of SB7-A to a lesser degree. However, even though the flowsheet value could mean an overestimate of the needed acid for nitrite destruction, an intermediate value of nitrite concentration, measured after 75% of the SRAT reflux had elapsed, yielded a small value of 472 mg/kg. This indicates that while the acid need of the blend simulant was overestimated by KMA, this is a negligible difference.

SB7 simulant processing presented few significant processing issues, regarding either chemical or physical properties. A very small amount of foaming was detected around the agitator shafts during SB7-2 (qualification, high acid) and SB7-5 (flowsheet, low acid) but controlling this foam behavior was not problematic. Also there were no instances of ammonia scrubber column flooding. Based on the SRAT or SME products, whether qualification and flowsheet, there should not be significant issues with mixing or transferring since the rheology was within DWPF limits.

A high oxalate qualification run was performed since part of the real SB7 waste originates from Tank 7 which, after the enhanced chemical cleaning, contains a significantly high concentration of oxalate. This increase of oxalate concentration did not cause any processing difficulties. However, there were two notable chemical effects: decreased hydrogen gas production and decreased mercury stripping. The latter suggests that oxalate could coordinate with mercury. Acid strike sample preparations were necessary to account for oxalate in the SRAT and SME product slurries using ion chromatography.

The performance of an extended run at the prototypical DWPF conditions (1 gallon per minute acid addition and 3,000 lb/h of steam) did not cause any significant problems or adverse changes in gas generation or rheology. The addition of simulated Actinide Removal Process (ARP) and Modular Caustic Side Solvent Extraction Unit (MCU) streams to the SRAT cycle did not influence the recommended acid stoichiometry recommendation.

The SRAT product samples indicated mercury limits were met except for the run with extended processing time, but the mercury balances were not fully closed. Up to 86% of the mercury was unaccounted for during runs with high acid stoichiometry. High mercury losses during tests at high acid stoichiometry have been noted during previous testing, including SB6 flowsheet testing. Unlike the Phase III SB6 high acid runs, there was no visible deposition of mercury or mercury amalgams on the agitator shaft or blades.

There was a significant amount of ammonium ion and ammonia generated as the pH rose above neutral during the SRAT cycles, as was the case for SB6. Secondary peak production of hydrogen, CO_2, and N_2O in the high acid runs with both the flowsheet and qualification simulants seem to coincide around the same time, suggesting that a common reactant may be involved in the production of these gases. The production of ammonia and ammonium is likely related to these precursor gases and there is speculation from the SB6 Phase III study that a possible mechanism for producing ammonia would involve a catalyst of either Ru or a mercury amalgam; there is no evidence here that would either support or discard these possibilities.

It is recommended that DWPF process SB7 at the following acid stoichiometry: 110% KMA or 112% Hsu. If the need should arise, increments of 5% in acid stoichiometry up to about 155% of the Hsu equation could be used in search for optimal processing.

Further study of the mercury chemistry in the CPC process is needed to evaluate the cause of mercury balance closure issues and to determine methods that could increase mercury stripping efficiency. Characterization of the products from this study is being pursued as part of the SRNL effort to understand mercury chemistry during DWPF processing.

TABLE OF CONTENTS

LIST OF TABLES

LIST OF FIGURES

LIST OF ABBREVIATIONS

ACTL	Aiken County Technology Laboratory
AD	Analytical Development
CPC	Chemical Process Cell
CS	Calcined Solids
CSTR	Continuous-Stirred Tank Reactor
DWPF	Defense Waste Processing Facility
FAVC	Formic Acid Vent Condenser
GC	Gas Chromatography
IC	Ion Chromatography
ICP-AES	Ion Chromatography-Atomic Energy Spectroscopy
IS	Insoluble Solids
MWWT	Mercury Water Wash Tank
PSAL	Process Science Analytical Laboratory
REDOX	Reduction/Oxidation Potential
SBx	Sludge Batch number x
SME	Slurry Mix Evaporator
SRAT	Sludge Receipt and Adjustment Tank
SRNL	Savannah River National Laboratory
SS	Soluble Solids
TS	Total Solids
TT&QAP	Technical Task and Quality Assurance Plan
TTR	Technical Task Request

1.0 Introduction

The Defense Waste Processing Facility (DWPF) will transition from Sludge Batch 6 (SB6) processing to Sludge Batch 7 (SB7) in fiscal year 2011. Tank 4, 7, and 12 material comprises the SB7 sludge. Tests were conducted using non-radioactive simulants of the expected SB7 compositions, both blend and qualification types, to determine the impact of varying the acid stoichiometry during the Sludge Receipt and Adjustment Tank (SRAT) and Slurry Mix Evaporator (SME) processes. The work was performed to meet the Technical Task Request (TTR) HLW-DWPF-TTR-2010-0012,[1] and the subsequent guidelines of a Task Technical and Quality Assurance Plan (TT&QAP) SRNL-RP-2010-0071.[2]

The primary justification for this work was to evaluate the acid window while measuring the impact of the acid addition on hydrogen gas generation as well as N_2O and CO_2 production. A notable difference of this batch is the high concentration of oxalate; the reason for this increase is that Tank 7, which is a major component of the feed to Tank 51/SB7 sludge, holds the material removed during oxalic acid chemical cleaning of Tanks 5 and 6[3-6]. Additional reasons for examining the behavior of SB7 were to understand the effects of combining a relatively high mercury level, ca. 2 wt%, and some of the highest noble metal (namely Rh and Ru) concentrations to date. Measurements included pH, off-gas, and mercury stripping profiles. For most of the runs, reflux and dewatering lasted about 24 hours at the scaled DWPF design maximum boil-up rate of 5,000 lb/h of steam; similarly acid addition was added at the scaled design rate of 2 gallon per minute. The flowsheet study included an "extended" run which operated at prototypical DWPF conditions, 1 gallon per minute of acid addition and a boil-up rate of 3,000 lb/h of steam.

2.0 Method

2.1 Experimental Method

These SRAT/SME experiments were performed in the SRNL facilities within the Aiken County Technology Laboratory (ACTL). As stated above, this study consisted of two types of runs, SB7-1 though SB7-4 for the qualification study and SB7-5 through SB7-9 for the flowsheet study; the experiments were conducted using two 4-L rigs.

Figure 1 shows a schematic of the SRAT apparatus. Details of the SRAT equipment are given in the equipment set-up memo[7] and details of the experimental procedures are given by Procedure ITS-00094, Rev. 3 from the L29 manual. However, information regarding a somewhat recent addition to the apparatus is discussed here. An ammonia gas absorption column (or ammonia scrubber) was added to the SRAT apparatus to collect ammonia in the off-gas for quantification of the generation rate and amount, and to protect the Nafion dryer. The ammonia scrubber used a solution of 749 g of de-ionized water and 1 g of 50 wt% nitric acid. This solution allowed for absorption of ammonia gas, yielding the aqueous ammonium cation, NH_4^+. The solution was circulated by a Micropump gear pump at about 300 mL per minute to a spray nozzle at the top of the packed section. The addition of the scrubber to the off-gas system slightly increased the back-pressure on the SRAT vessel and led to a small increase in fugitive emissions at the various fittings; thus, water vapor loss increased as well.

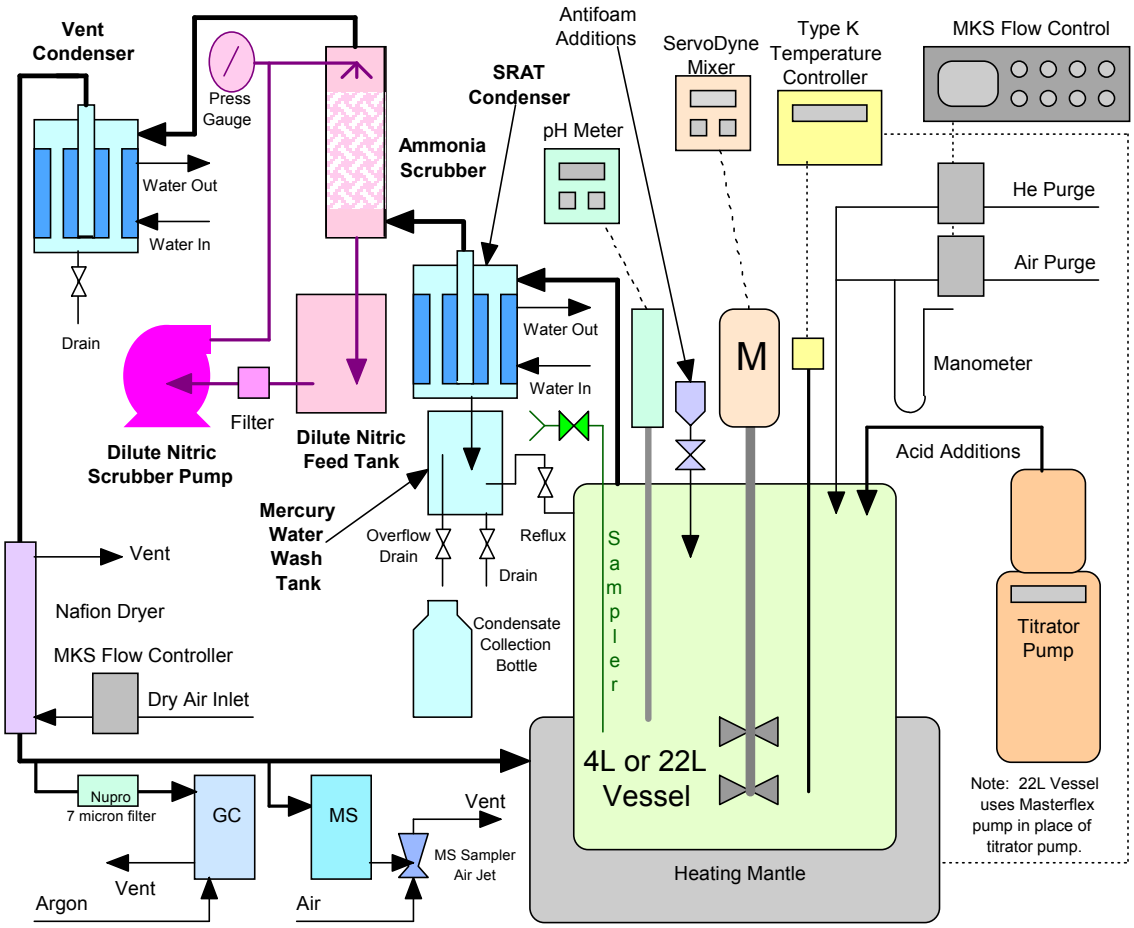

Figure 1 Schematic of SRAT/SME Apparatus

The automated data acquisition system developed for the 4-L SRAT rigs was used to collect electronic data on a computer. Process variable data included SRAT slurry temperature, bath temperatures for the cooling water to the SRAT condenser and Formic Acid Vent Condenser (FAVC), slurry pH, SRAT mixer speed and torque, and air and helium purge flows (helium is used as an internal standard set to 0.5% of the nominal SRAT purge air flow). Cumulative acid addition volume data were collected from the automated dispensers using an algorithm that matches the indicated total on the dispenser. Some pH data were obtained for the nitric acid reservoir that supplied the reflux flow to the ammonia scrubbers.

Raw GC data were acquired on separate computers dedicated to each instrument. The chilled off-gas leaving the FAVC was passed through a Nafion dryer in counter-current flow with a dried air stream to reduce the moisture content at the GC inlet. Agilent 3000A micro GCs were used on both runs. The GCs were baked out before the runs. Column-A can collect data related to He, H_2, O_2, N_2, NO, and CO, while column-B can collect data related to CO_2, N_2O, and water. GC's were calibrated with a standard calibration gas containing 0.500 vol% He, 1.000 vol% H_2, 20.00 vol% O_2, 51.50 vol% N_2, 24.50 vol% CO_2 and 2.50 vol% N_2O. The calibration was verified prior to

starting the SRAT cycle and after completing the SRAT cycle. Room air was used to give a two point calibration for N_2.

2.2 Sample Analysis

Chemical and physical measurements of samples of off-gas and condensed media, both supernate and slurry have been performed. The chemical measurements consisted of analyzing samples for pH and composition values while the physical measurements consisted of rheology and density measurements.

Process samples were analyzed by various methods. Slurry and supernate elemental compositions were determined by inductively coupled plasma-atomic emission spectroscopy (ICP-AES) at the Process Science Analytical Laboratory (PSAL). Slurry samples were calcined at 1100°C. The main advantage of this approach is to permit easier comparisons between SRAT product elements and sludge elements. Noble metals and mercury are trimmed uniquely to each SRAT, and their concentrations are known more accurately from material balance considerations than they could be from ICP-AES analyses. Dewatering condensate samples were sent to PSAL to check for dissolved mercury via ICP-AES.

Water soluble anions were determined by PSAL using ion chromatography (IC) on 100-fold weighted dilutions of slurry followed by filtration to remove the remaining insoluble solids. Oxalate was analyzed by AD using IC following an acid strike to dissolve insoluble oxalate compounds followed by water dilution. Ammonium ion concentrations were measured from samples of SRAT cycle slurries, SRAT product slurries, SRAT cycle condensates, and ammonia scrubber liquids (see above for scrubber description) by AD using IC. The starting sludge was titrated to pH 7 using the PSAL auto-titrator to determine the base equivalents for input into the stoichiometric acid equation.

Ammonia and mercury gas concentrations at the SRAT condenser exit were measured via a Sensidyne colorimetric gas detector tube system. Gas measurements were performed in the second half of the SRAT reflux period since NO_x, present to a larger degree during acid addition, dewatering, and earlier in the SRAT reflux period, interferes with the colorimetric tube performance.

Slurry and supernate densities were measured by PSAL using the Anton-Parr DMA 4J70 instrument. A Mettler halogen lamp solids analyzer was used to obtain the total solids, soluble solids, and insoluble solids weight percents.

Slurry rheology measurements were obtained by using a Haake RS-600 rheometer with the Z41 concentric cylinder geometry (SRAT product) and Z38 cylinder (SME product).[8] The rheometer uses a Searle type measuring system, where both speed and torque are measured at the rotating shaft. This was operated in the controlled rate mode for all of the data reported here. Flow curves were obtained by varying the shear rate from 0 to 600 seconds^{-1} (SRAT products) or 0 to 300 seconds^{-1} (SME products) over a given time period; measurements of the shear stress were obtained from the torque on the rotating shaft.

2.3 Simulant Preparation and Composition

Both simulants, SB7-Q for the qualification studies and SB7-A for the flowsheet work, were prepared using the current continuous stirred reactor (CSTR) precipitation method.[9] The method involved the following steps

a. precipitated MnO_2 was added
b. metal nitrate solution was prepared
c. these two were combined along with a 50% sodium hydroxide solution to produce a caustic slurry of hydrous metal oxide and insoluble hydroxides in a sodium nitrate solution at pH~9.5
d. sodium carbonate was added to convert some hydroxides to carbonates
e. the slurry was washed and decanted until the nitrate concentration was below the target supernate nitrate concentration
f. concentration allowed for attainment of the target total solids value
g. silica and titanium oxide were added to complete the raw sludge
h. soluble sodium salts were added to bring the supernate composition to target values

Table 1 lists some selected analyses for various sludge batches. There are six Shielded Cell (SC) sets of data, the last four of which are labeled as such by run number, e.g. SC-3. The SC-11 column refers to the Cells work performed on the SB7 qualification sample from Tank 51.[10] The SB6-G column refers to the simulant blend while the last two columns refer to the present simulant work used for the qualification and blend CPC simulations of SB7. The weight percent of Mn is on a calcined solids basis while those for mercury and the noble metals are on a total solids basis. SB7 has a moderately high mercury level, about 2% of the total solids, close to that of SB5 but less than SB6, which was about 3%. The key noble metals concentrations are elevated by about 10-20% relative to those of SB6.

Table 1 – Comparison of Various Real Washed Sludges to SB6 and SB7 Simulants§

	SB2[11] (SC)	SB3[12] (SC)	SB4[13] (SC-3)	SB5[14] (SC-6)	SB6[15] (SC-9)	SB6-G[15] Blend	SB7[10] (SC-11)	SB7-Q QUAL	SB7-A Blend
Wt% TS	18.4	27.2	19.5	17.1	15.1	17.8	18.1	18.0	18.5
Wt% IS	15.0	17.1	16.5	11.2	9.9	10.9	12.3	12.6	13.0
Wt% SS	3.4	10.1	3.0	5.9	5.2	6.9	5.8	5.4	5.4
Wt% CS	15.7	N/A	16.6	14.0	11.9	13.9	13.3	13.6	13.6
Base, M	0.308	0.577	0.316	0.739	0.58	0.839	0.38	0.615	0.580
TIC†	866	1,260	2,510	1,280	913	1,050	912	1,380	1,180
Nitrite†	7,529	25,300	20,500	8,660	10,000	13,950	9,900	9,140	9,600
Mn, wt%	3.21	3.98	1.94	3.66	4.15	4.82	4.26	4.37	5.12
Hg, wt%	0.195	0.0654	2.57	2.2	3.12	2.79	1.5	1.94	2.16
Ag, wt%	0.0107	0.0136	0.0036	0.0135	0.0138	0.0142	0.0132	0.0172	0.0164
Pd, wt%	0.0009	0.0017	0.0010	0.0040	0.0030	0.0028	0.0026	0.0041	0.0038
Rh, wt%	0.0078	0.0071	0.0124	0.0250	0.0187	0.0177	0.0188	0.0233	0.0219
Ru, wt%	0.0332	0.0362	0.0529	0.110	0.0924	0.0846	0.0902	0.1053	0.1000
Acid‡	0.751	1.63	1.30	1.32	1.12	1.49	1.05	1.30	1.33

§ TS, IS, SS, and CS mean total solids, insoluble solids, soluble solids, and calcined solids.
† mg/kg slurry

Table 2 shows the slurry and supernate density and anion levels of the sludges. Note that the nitrite level is significantly lower in SB7, compared to SB6. As a side note, there is less chlorine in SB7 which could preclude some reactions with mercury to produce mercuric chloride ($HgCl_2$) and mercurous chloride (calomel, Hg_2Cl_2); however, a small amount of chlorine is introduced upon trimming with $RuCl_3$ in the simulant testing. Since the ratio of mercury to chlorine atoms is 8.0 and 9.3 for the qualification and flowsheet runs, respectively, it is not likely that chlorine has a dominant impact on mercury chemistry; however a possibility could include catalysis.

Table 2 - Anion composition and density of SB7-Q and SB7-A

	SB6-G Blend	**SB7 (SC-11)**	**SB7-Q Qual**	**SB7-A Blend**
Nitrite, mg/kg	13,950	9,900	9,140	9,610
Nitrate, mg/kg	8,030	7,900	6,465	5,880
Sulfate, mg/kg	1,820	2,100	1,460	1,350
Chloride, mg/kg	244	< 400	< 100	< 100
Oxalate, mg/kg	600	8,100	10,000	8,170
Slurry TIC, mg/kg slurry	1,050	910	1,380	1,180
Supernate TIC, mg/kg supernate	920	870	660	760
Slurry density, g/mL	1.149	1.150	1.142	1.144
Supernate density, g/mL	1.062	1.05	1.053	1.051

Two preparation methods, acid strike and weighted dilution with water, gave essentially identical results for the SB7 simulant oxalate which was introduced as sodium oxalate. SB7-4 was trimmed with an additional 8,395 mg oxalate/kg prior to the SRAT cycle.

Table 3 lists the calcined elemental composition of both sludges and allows for comparison with the previous sludge SB6-G; the units are wt% on a calcined basis. Note that the differences in composition are not great.

Table 3 - Elemental Calcined wt% of SB7-Q and SB7-A Simulants (1100 °C)

Element	SB6-G Blend wt %	SB7 (SC-11) wt %	SB7-Q Qual wt %	SB7-A Blend wt %
Al	13.0	14.4	15.7	15.9
Ba	0.13	0.12	0.10	0.11
Ca	0.63	0.76	0.83	0.83
Ce	0.20	0.16	0.15	0.16
Cr	0.17	0.058	0.05	0.06
Cu	0.10	0.053	0.03	0.05
Fe	20.6	18.0	19.2	19.9
K	0.08	0.088	0.13	0.12
La	0.10	0.07	0.07	0.08
Mg	0.50	0.38	0.37	0.41
Mn	6.2	4.26	4.37	5.12
Na	17.6	19.0	15.3	14.7
Ni	2.8	3.1	3.4	3.3
P	<0.1	0.087	<0.1	<0.1
Pb	<0.01	0.04	0.03	0.02
S	0.39	0.52	0.37	0.33
Si	1.26	2.01	1.91	1.87
Ti	0.03	0.02	0.03	0.03
Zn	0.09	0.04	0.05	0.06
Zr	0.26	0.16	0.25	0.25

Table 4 lists the elemental supernate concentrations in mg/L compared to those in the SB6 flowsheet simulant.

Table 4 - Elemental Concentrations of SB7-Q and SB7-A Supernates

Element	SB6-G Blend, mg/L	SB7-Q Qual, mg/L	SB7-A Blend, mg/L
Al	3,600	2,460	2,130
Ba	< 0.1	< 0.1	< 0.1
Ca	5.85	2.38	2.33
Ce	< 10	< 0.1	< 0.1
Cr	52.4	6.34	17.4
Cu	< 1	0.414	0.343
Fe	< 0.1	< 0.1	< 0.1
K	280	160	129
La	< 0.1	< 0.1	< 0.1
Mg	< 0.1	< 0.1	< 0.1
Mn	< 0.1	< 0.1	< 0.1
Na	n.m.	23,850	20,600
Ni	< 0.1	< 0.1	< 0.1
P	< 10	< 10	< 10
Pb	< 0.1	< 0.1	< 0.1
S	975	763	706
Si	2.20	0.685	0.423
Sn	0	1.32	2.36
Ti	< 0.1	< 0.1	< 0.1
Zn	< 0.1	< 0.1	< 0.1
Zr	< 0.1	< 0.1	< 0.1

n.m. – not measured

3.0 Results and Discussion

Two sets of SRAT/SME simulations were performed, qualification and flowsheet. The qualification studies reflect the behavior of the SB7 sludge as prepared in Tank 51 and targets the composition of the sludge used during Shielded Cells qualification testing, while the flowsheet work models the behavior of SB7 processing after the initial mixing with the SB6 heel in Tank 40. The discussion covers the qualification testing results first, followed by the flowsheet results.

3.1 Qualification CPC Simulation

Four SRAT/SME simulations were performed for the qualification portion of this work. These runs were labeled SB7-1 through SB7-4. Table 5 shows the acid stoichiometric factors and total acid added per liter of starting sludge simulant. The two acid equations are discussed in detail elsewhere.[16] The Hsu equation is the one currently used by DWPF. The SB7-4 high oxalate run consisted of increasing the oxalate concentration by 8,395 mg/kg relative to the other three tests. The values for the Shielded Cells qualification test, SC-11, are given for comparison.

Table 5 - Qualification Run Acid Levels

Run ID - Function	Total Acid, mol/L	Hsu factor	KMA† factor
SB7-1 - Low acid	1.18	103%	100%
SB7-2 - High acid	1.78	146%	150%
SB7-3 - Baseline	1.30	107%	110%
SB7-4 - High Oxalate	1.30	107%	110%
SC-11*	1.05	118%	110%

† Koopman minimum acid equation
* SC-11 pertains to SB7/Tank 51 qualification sample demonstration

SB3 studies showed acid consumption increased with increasing oxalate concentration; sodium oxalate was the compound used to introduce the oxalate into the sludge. Current stoichiometric acid equations, however, do not adjust the calculated acid demand for oxalate. Therefore, it was expected that increasing the oxalate would cause a decrease in excess acid. Oxalate is accounted for in the predicted glass redox calculations.

3.1.1 *Qualification Elemental/Ion Analyses*

The following ten tables (Table 6 through 15) show general properties, anion concentrations, and elemental concentrations of the SRAT and SME products. Figure 14, in the Appendix, shows some additional data, as well as the pH profiles of the qualification runs. The nitrite concentration measured for the low acid (100% Koopman minimum acid) run is of interest; Table 8 shows that this value is 760 mg/kg slurry, which is just slightly below the nominal target of <1,000 mg/kg. Thus, the Koopman minimum acid equation accurately predicted the amount of acid necessary to effectively destroy nitrite. The anion chemistry, Table 9, shows no unusual behavior.

Another noteworthy feature is that the high acid run exhibits the lowest mercury concentration in the slurry, about a third of the other three runs; this is true for both the SRAT and SME products. This behavior parallels the unusually rapid decreases of the mercury-time profiles of SB6-G sludge high acid runs.[17] Section 3.1.4 and Section 3.2.4 will show similar profiles for tests with SB7-Q and SB7-A sludges. Note that in Table 8 the intermediate values of nitrite concentration were measured for the baseline and high oxalate runs (but not for the low and high acid runs).

Table 6 - Properties of Qualification SRAT Products

	SB7-1 Low Acid	SB7-2 High Acid	SB7-3 Baseline Acid	SB7-4 High Oxalate
Wt% Total Solids	25.2	23.5	24.5	24.8
Wt% Insoluble Solids	16.1	14.7	14.6	14.5
Wt% Soluble Solids	9.1	8.8	8.9	10.3
Wt% Calcined Solids	17.5	16.2	17.1	16.5
Slurry density, g/mL	1.16	1.17	1.16	1.20
Supernate density, g/mL	1.08	1.07	1.08	1.08
pH at 25°C	8.0	8.8	8.9	8.7
Wt% Hg, dried solids basis †	0.070	0.024	0.072	0.062

† The mercury concentrations are potentially non-representative (see Section 3.1.4).

The next table gives the anion concentrations found in the dewatered condensate collected following formic acid addition.

Table 7 - Qualification SRAT Dewater Anions

	SB7-1 Low Acid	SB7-2 High Acid	SB7-3 Baseline Acid	SB7-4 High Oxalate
Nitrite, mg/L	220	< 100	116	< 100
Nitrate, mg/L	3,250	701	3,450	3,410
Formate, mg/L	292	3,075	293	174
Sulfate, mg/L	< 100	< 100	< 100	< 100
Chloride, mg/L	< 100	< 100	< 100	< 100

SRAT product slurry anion results are given in Table 8. "Intermediate values" of nitrite were measured after about 75% of the SRAT reflux period had elapsed. These values represent lower bounds, since the samples were not caustic quenched to stop acid driven reactions such as nitrite destruction.

Table 8 - Qualification SRAT Product Anions

	SB7-1 Low Acid	SB7-2 High Acid	SB7-3 Baseline Acid	SB7-4 High Oxalate
Intermediate Nitrite†	n.m.	n.m.	< 100	612
Nitrite, mg/kg	760	< 100	< 100	175
Nitrate, mg/kg	24,700	24,800	25,400	27,700
Formate, mg/kg	36,900	35,400	38,500	35,100
Sulfate, mg/kg	1,930	1,815	1,715	1,925
Chloride, mg/kg	259	194	263	235

† Intermediate values of NO_2^- concentration during reflux
n.m. – not measured

Most of the anion results were about as expected. The SB7-2 formate indicated fairly high formate destruction, since it received the most formic acid yet had less formate than the low acid and baseline acid SRAT products.

SRAT oxalate values are not listed, because the method involving weighted dilution with water was not effective at dissolving certain insoluble oxalate species such as calcium oxalate. Attempts to use the acid spike method at PSAL,[18] the same method used in SB3 flowsheet studies, to obtain more accurate oxalate concentrations, yielded values that were about twice the expected concentrations based on the feed concentrations. In retrospect, the SB3 work may have occasionally suffered from somewhat similar problems.[19]

SB7-4 nitrite levels relative to the baseline run seem to indicate that increasing the oxalate diminished the rate of nitrite destruction. It will be seen in a later section that the high oxalate run also exhibited lower hydrogen generation rates. It can be concluded that the increased oxalate concentration consumed some of the excess acid present in SB7-4 causing both the slower nitrite destruction and the reduced hydrogen generation rates.

Table 9 - Qualification SRAT Anion Reactions

	SB7-1 Low Acid	SB7-2 High Acid	SB7-3 Baseline Acid	SB7-4 High Oxalate
Nitrite Loss %	93%	100%	100%	98%
Net Nitrite-to-Nitrate %	20%	-20%	14%	11%
Formate Loss %	25%	50%	26%	24%
Formate Lost, g	35	104	39	34

SB7-2 had "negative" nitrite-to-nitrate conversion indicating an actual net loss in nitrate ion relative to the nitrate in the feed slurry and added nitric acid. This condition often coincides with ammonium ion formation later in the SRAT cycle.

Table 10 - Calcined Elemental Composition, wt%, of SRAT Products (1100°C)

Element	SB7-1 Low Acid	SB7-2 High Acid	SB7-3 Baseline Acid	SB7-4 High Oxalate
Al	15.9	16.0	15.6	15.2
Ba	0.12	0.11	0.10	0.09
Ca	0.86	0.87	0.81	0.80
Ce	0.14	0.14	0.15	0.14
Cr	0.05	0.05	0.05	0.05
Cu	0.04	0.03	0.05	0.04
Fe	19.1	19.2	19.3	18.0
K	0.12	0.12	0.11	0.12
La	0.07	0.07	0.07	0.07
Mg	0.35	0.35	0.38	0.34
Mn	4.3	4.2	4.38	4.22
Na	15.9	16.1	15.7	17.4
Ni	2.8	2.72	3.42	3.21
Pb	0.03	0.028	0.02	< 0.01
Rh	< 0.1	< 0.1	< 0.1	< 0.1
Ru	< 0.1	< 0.1	< 0.1	< 0.1
S	0.39	0.40	0.40	0.37
Si	2.1	2.1	1.83	1.75
Ti	0.03	0.03	0.04	0.04
Zn	0.05	0.05	0.05	0.04
Zr	0.25	0.25	0.25	0.23

The SRAT product elemental data confirm essentially consistent batching of the lab-scale SRAT for the four process simulations. The nickel results in SB7-1 and 2 appear to be off low by more than 10% compared to the analyzed composition of the feed sludge and the results for SB7-3 which matched those of the feed sludge analysis. SB7-4 results are lower than the others, except for sodium, due to the extra sodium oxalate addition. The expected increase in sodium was roughly 3% (15.3 to 18.6%), but the measured increase was smaller. Rh and Ru recoveries in calcined solids are typically less than 20% of the amounts trimmed into the SRAT feed.

SRAT product supernate concentrations for the elements are given in Table 11.

Table 11 - Elemental Composition SRAT Product Supernate

Element	SB7-1 Low Acid mg/L	SB7-2 High Acid mg/L	SB7-3 Baseline Acid, mg/L	SB7-4 High Oxalate mg/L
Al	1.69	1.81	1.55	1.13
B	2.09	5.85	1.89	1.19
Ca	17.9	9.34	9.65	4.46
Ce	0.384	0.344	0.400	0.457
Cr	< 0.1	< 0.1	< 0.1	< 0.1
Cu	0.874	0.848	0.163	0.598
Fe	< 0.1	< 0.1	< 1	< 1
K	483	418	436	395
Li	< 0.1	< 0.1	< 10	< 10
Mg	60.7	112	113	39.8
Mn	328	486	845	667
Ni	3.40	1.91	3.35	43.6
S	789	785	871	991
Si	19.5	29.2	15.0	13.0
Sn	0.508	0.499	0.785	0.759
Ti	< 0.1	< 0.1	0.193	0.169
Zn	< 0.1	< 0.1	< 0.1	< 0.1
Zr	< 0.1	< 0.1	< 0.1	< 0.1

Ca and Mg, which are frequently found at concentrations over 1,000 mg/L in other SRAT tests, were barely soluble in any of the SRAT products. The key observation for Table 11 was that very little sludge was dissolved in these runs compared to runs with minimal oxalate. Comparison of the SRAT supernate product concentrations of the baseline and high oxalate runs in Table 11 reveals further decreased Ca, Mg, and Mn concentrations in the high oxalate run and slightly greater Ni concentration. It would appear that the oxalate is causing Ca, Mg and Mn to form insoluble compounds either directly by attachment to oxalate or indirectly with some other anion. The reason for the enhancement of Ni solubility is not known but may be due to the 0.3 unit lower pH value of SB7-4.

The following tables give similar properties of the four SME products.

Table 12 - Properties of Qualification SME Products

	SB7-1 Low Acid	SB7-2 High Acid	SB7-3 Baseline	SB7-4 High Oxalate
Wt% Total Solids	49.8	47.7	48.1	48.5
Wt% Insoluble Solids	41.3	39.3	39.3	39.1
Wt% Soluble Solids	8.6	8.4	8.8	9.5
Wt% Calcined Solids	43.0	41.1	41.7	41.4
Slurry density, g/mL	1.43	1.40	1.42	1.40
Supernate density, g/mL	1.10	1.10	1.10	1.10
pH at 25°C	7.7	8.2	8.3	8.4
Wt% Hg, dried solids basis	0.020	0.014	0.035	0.037

It is interesting to note that the low acid run managed to end up with the lowest pH of the four. This counter intuitive trend is apparently linked to the catalytic destruction of formic acid in higher acid runs that can actually exceed the amount of additional acid being added leading to less residual acid in the SME product.

Table 13 - Qualification SME Product Anions

	SB7-1 Low Acid	SB7-2 High Acid	SB7-3 Baseline	SB7-4 High Oxalate
Nitrite, mg/kg	372	< 100	< 100	< 100
Nitrate, mg/kg	21,150	22,000	20,950	24,800
Formate, mg/kg	34,100	33,850	33,850	33,750
Sulfate, mg/kg	1,860	1,720	1,525	1,740
Chloride, mg/kg	272	216	234	216
Oxalate, mg/kg	n.m.	n.m.	10,400	17,900

n.m. – not measured

Limited effort was put into the qualification simulant SME oxalate determinations by the acid strike method. The AD IC was used to make these measurements. SB7-3 and 4 were selected to evaluate the impact of spiking oxalate on the SME product oxalate. Calculated oxalate loss by material balance was small for both runs: 3% for SB7-3 and 6% for SB7-4. These results are in the noise of the analytical results for oxalate which had standard deviations of 8% of the measured values. The measured increase from -3 to -4 was quite close to the amount expected from the spiked sodium oxalate in SB7-4.

The SME elemental data for both the calcined and supernate phases are given in Table 14 and Table 15. Frit 418 was used in all four simulations. The actual waste loading by material balance for all four qualification runs varied from 35.4% to 35.7%. These values agree well with the target waste loading of 36%. The difference was due to cumulative SRAT sample masses being somewhat larger than predicted prior to the runs.

Table 14 - Calcined Elemental Composition, wt%, of SME Products (1100 °C)

Element	SB7-1 Low Acid	SB7-2 High Acid	SB7-3 Baseline	SB7-4 High Oxalate
Al	5.94	6.15	6.09	5.74
B	1.42	1.44	1.49	1.41
Ba	0.046	0.045	0.039	0.036
Ca	0.460	0.392	0.351	0.334
Ce	0.043	0.045	0.052	0.048
Cr	0.035	0.037	0.033	0.027
Cu	0.036	0.034	0.024	0.037
Fe	6.99	6.93	6.95	6.49
K	0.085	0.079	0.078	0.076
La	0.028	0.029	0.023	0.022
Li	2.19	2.25	2.22	2.19
Mg	0.143	0.152	0.152	0.140
Mn	1.42	1.49	1.58	1.45
Na	9.87	9.81	9.52	9.99
Ni	1.13	1.18	1.22	1.17
Pb	0.014	0.012	0.012	0.012
Rh	< 0.1	< 0.1	< 0.1	< 0.1
Ru	< 0.1	< 0.1	< 0.1	< 0.1
S	0.175	0.142	0.118	0.124
Si	23.5	24.0	23.9	23.7
Ti	0.064	0.068	0.061	0.054
Zn	0.026	0.035	0.019	0.018
Zr	0.192	0.195	0.185	0.174

The SB7-1 and 2 slurry nickel values fell in line with those for SB7-3 in spite of the measured differences in the SRAT products. The SME product calcined elemental value for SB7-4 sodium is only slightly higher than those of the other runs; this was also the case for the SRAT products. The reasons for this are unknown, since the sodium oxalate addition to SB7-4 should have produced an increase of roughly one percent compared to SB7-1 through 3 (9.7% to 10.9%).

Table 15 - Elemental Composition of Qualification SME Supernate Products

Element	SB7-1 Low Acid mg/L	SB7-2 High Acid mg/L	SB7-3 Baseline Acid, mg/L	SB7-4 High Oxalate mg/L
Al	1.76	1.61	1.26	1.55
B	35.3	17.2	13.6	41.6
Ca	32.3	30.7	16.43	5.33
Ce	1.53	1.51	0.604	1.14
Cr	< 0.1	< 0.1	< 0.1	< 0.1
Cu	1.626	0.857	0.263	0.278
Fe	< 0.1	< 0.1	< 1	< 1
K	615	595	550	504
Li	< 0.1	< 0.1	244	327
Mg	177	232	151	32.7
Mn	1,760	1,860	1,210	930
Ni	21.20	7.10	6.70	38.4
Rh	< 1	< 1	< 1	1.32
Ru	< 1	< 1	< 1	< 1
S	1,080	1,230	1,220	1,250
Si	21.6	38.6	18.1	17.3
Sn	2.70	2.40	1.40	1.24
Ti	< 0.1	< 0.1	0.182	0.166
Zn	< 0.1	< 0.1	< 0.1	< 0.1
Zr	< 0.1	< 0.1	< 0.1	< 0.1

Mn concentrations increased in the SME product supernate relative to the SRAT product supernate, but the total supernate mass decreased so there was not a large change in the amount of dissolved Mn. The SME supernate data agree with the SRAT data in indicating that very little of the initially insoluble sludge species were dissolved during processing.

3.1.2 *Qualification GC Results*

The qualification runs did not exceed hydrogen peak generation rate limits, 0.65 and 0.223 lb/h for the SRAT and SME cycles, respectively. Table 16 shows the peak gas generation rates as measured by the GC during the SRAT cycles. More detailed GC time profiles are shown in Figures 2, 3, and 4. Since these figures are congested and do not show the SME data clearly, SME-only data are given in the Appendix; see Figures 16-18. Hydrogen production was highest for the highest acid run, as expected. The next highest producer of hydrogen was the baseline run, at 110% acid level. The high oxalate run produced less hydrogen than the baseline. All runs exhibit similar peak CO_2 rates. The nitrous oxide rates are similar and relatively high for the high acid and baseline runs but are low for the low acid and high oxalate cases. Based on the behavior of SB7-4, less hydrogen generated and less nitrite destroyed, it is apparent that oxalate consumes acid.

Table 16 - Maximum SRAT Gas Generation Rates

Gas	SB7-1 Low Acid	SB7-2 High Acid	SB7-3 Baseline Acid	SB7-4 High Oxalate
H_2, lb/h	0.00	0.52	0.034	0.00
N_2O, lb/h	19.1	29.5	30.8	18.4
CO_2, lb/h	543	545	490	509

Table 17 contains the SME gas generation rates. The SME hydrogen generation trends are similar to those of the SRAT: greatest value from the high acid run and the lowest from the low acid and high oxalate cases. However, there is more variation in CO_2 and N_2O production (than in the SRAT cycle). SME CO_2 reflects catalytic activity, while SRAT CO_2 peaks are generally due to TIC destruction and tend to be fairly similar. The high acid run yielded the greatest CO_2 generation while the low acid and high oxalate runs yielded the least. N_2O production was different in that the high acid run produced none of the gas while the high oxalate and baseline runs produced the most. The lack of N_2O may indicate active ammonium ion formation in the SB7-2 SME cycle. Ammonium ion formation is a series of reactions which at intermediate points can release nitrite ion back into solution which gets converted into N_2O. There was also residual nitrite in the SB7-1 and -4 SRAT products that was destroyed in the SME cycle.

Table 17 - Maximum SME Gas Generation Rates

Gas	SB7-1 Low Acid	SB7-2 High Acid	SB7-3 Baseline	SB7-4 High Oxalate
H_2, lb/h	0.002	0.18	0.14	0.02
N_2O, lb/h	0.35	0.00	1.10	0.87
CO_2, lb/h	22.2	134	48.3	22.6

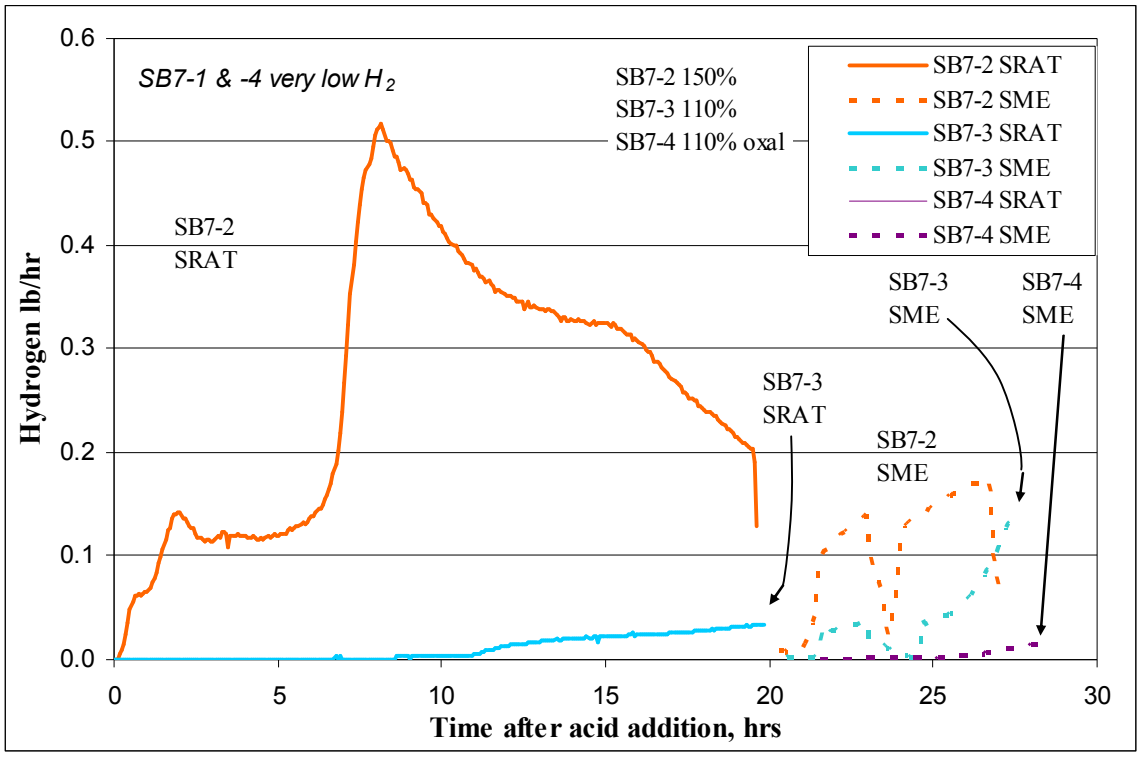

Figure 2 - Qualification SRAT/SME Hydrogen Profiles

Both CO_2 and N_2O production are greater in the high acid run, Figures 3 and 4. The secondary humps between 5 and 10 hours after the end of acid addition coincide for all three gases.

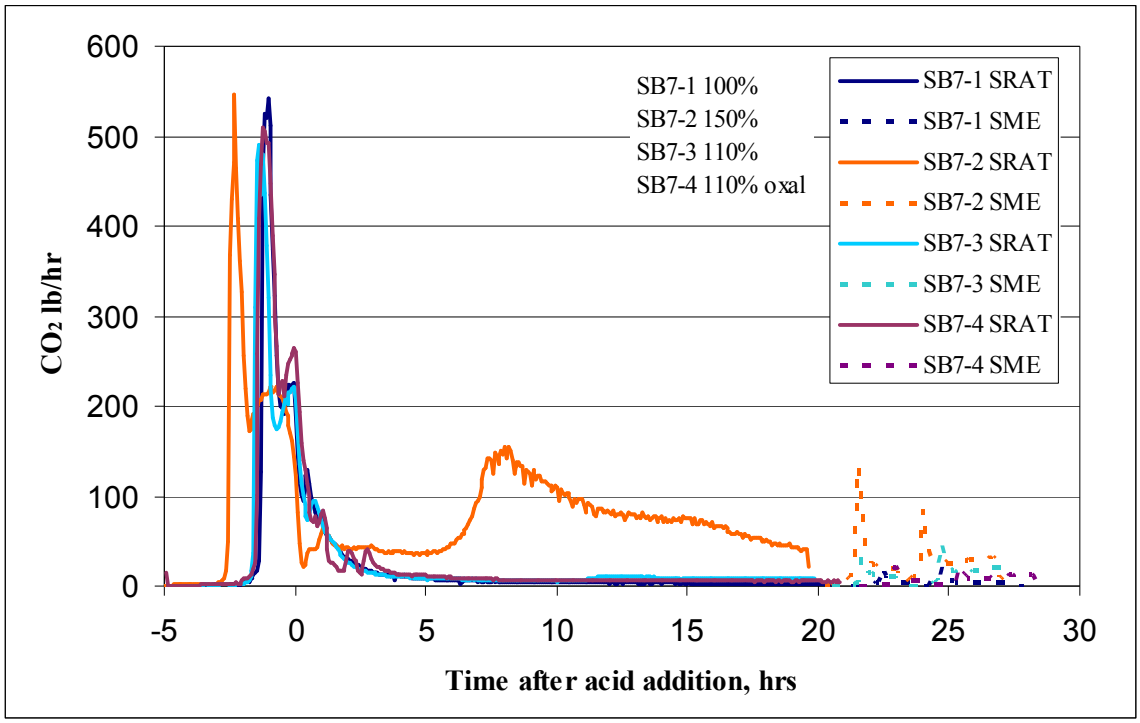

Figure 3 - Qualification SRAT/SME CO_2 Profiles

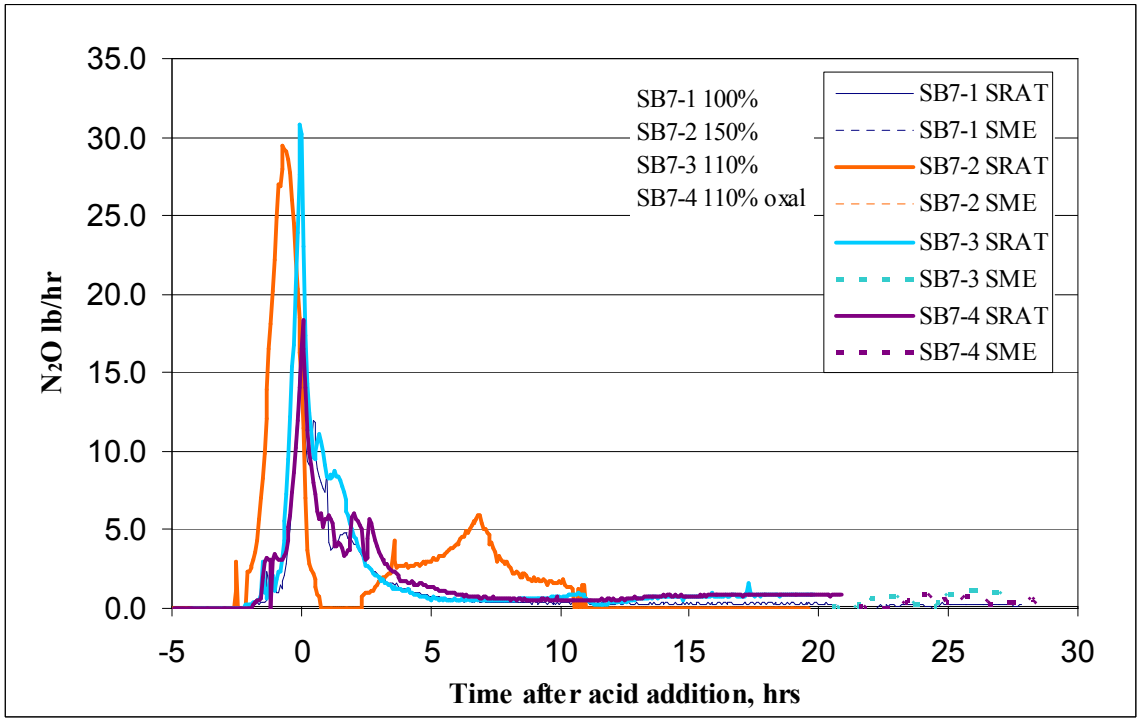

Figure 4 - Qualification SRAT/SME N_2O Profiles

3.1.3 *Qualification Ammonia/Ammonium Results*

The available data of ammonia and ammonium generation, the former measured at the outlet of the SRAT condenser and the latter captured in the ammonia scrubber liquid, are sparse but nonetheless indicate that limited excess acid tends to inhibit generation of these two species. The gas measurement of the baseline run was performed at an earlier time than the others but there is likely to be little interference from NO_x since the GC data in Figure 4 shows that the N_2O concentration was low after five hours of reflux.

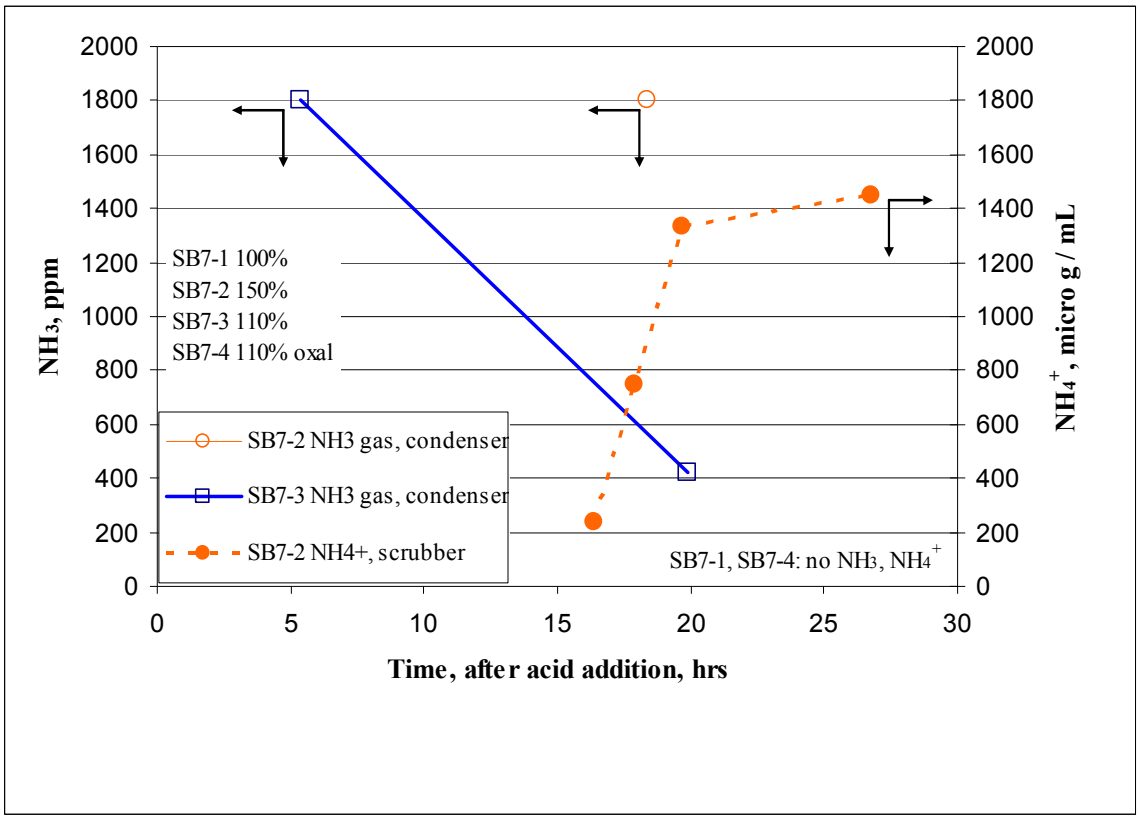

Figure 5 - Qualification SRAT Ammonia and Ammonium Concentrations

3.1.4 *Qualification Mercury Results*

The concentration of mercury was measured via the sample taken from in the SRAT/SME kettle and in the gas phase at the outlet of the SRAT condenser; the MWWT was also used to collect Hg. Mercury concentrations in the SRAT and SME product slurries are tabulated; see Table 18.

Table 18 - Mercury Composition in Qualification SRAT/SME Slurries

	SB7-1 Low Acid	SB7-2 High Acid	SB7-3 Baseline Acid	SB7-4 High Oxalate
SRAT product, Wt% Hg, dried solids	0.070	0.024	0.072	0.062
SME product, Wt% Hg, dried solids	0.020	0.014	0.035	0.037

Figure 6 shows the Hg time profile of all four qualification slurries; the same amount of mercury was trimmed into each of the runs. Note that the first values at the end of acid addition refer to a slurry before dewatering and thus are dilute relative to the rest of the data which correspond to SRAT sampling after dewatering was completed. The high acid run, SB7-2, shows a sudden drop in mercury concentration, consistent with SB6 high acid behavior.[17] The SB7-3 reading of 3500 at about 10 hours after formic acid addition may be an instance where a modest-sized bead of mercury was captured by the sample tube indicating heterogeneity in the distribution of mercury in the SRAT slurry.

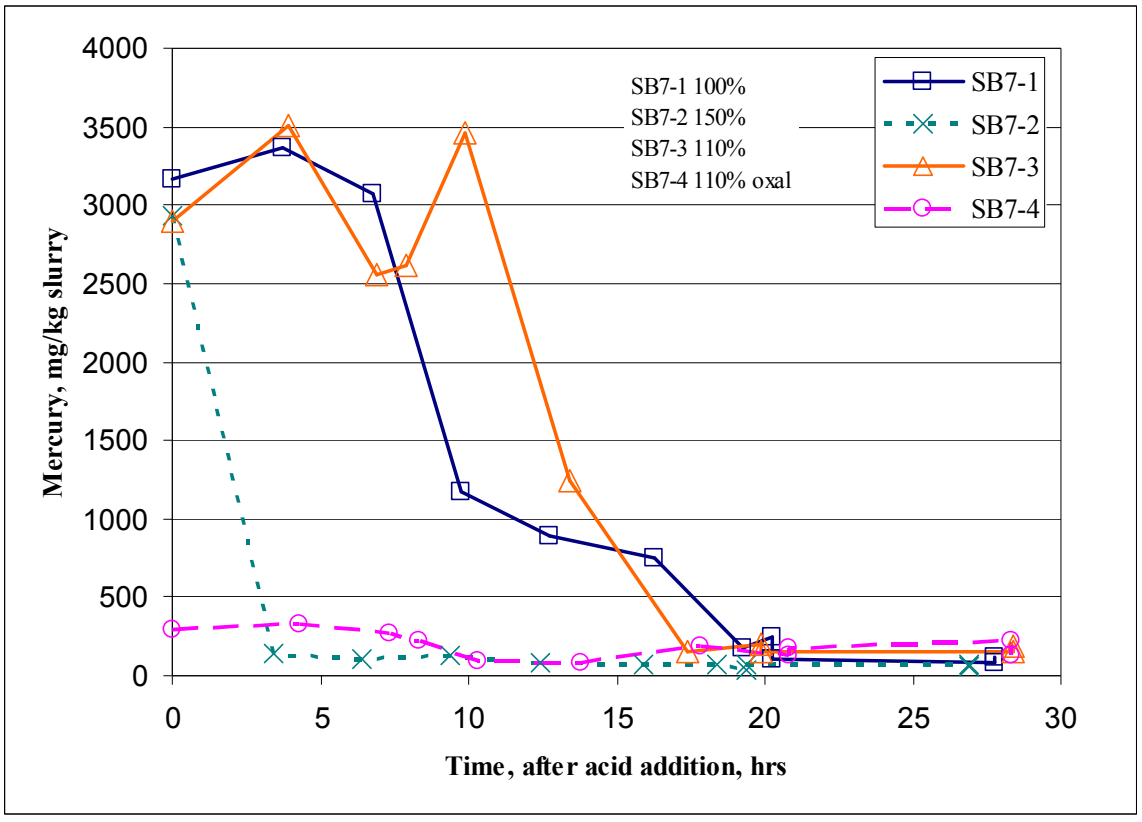

Figure 6 - Qualification Slurry Mercury Measurements

The behavior of mercury in the high oxalate run, SB7-4, is puzzling; the initial concentration of mercury in the slurry of the high oxalate run is anomalously low. It should be about ten times greater given that the same mass of mercuric oxide was added as in the other three runs. The reason for this very low mercury concentration after the end of acid addition could be associated

with the increase of oxalate which could catalyze the production and agglomeration of elemental mercury. Little was learned about the interactions between oxalate and mercury during the Sludge Batch 3 (SB3) testing, because SB3 sludge had a very low mercury concentration in the starting sludge, about thirty times less than the current mercury level.

Mercury gas measurements are shown in Figure 7; these measurements are too sparse to provide additional information than what is already shown in Table 6, low acid and high oxalate tend to decrease Hg concentration in the kettle. The gas measurement of the baseline run was performed at an earlier time than the others but there is likely to be little interference from NO_x since the GC data in Figure 4 shows that the N_2O concentration was low after five hours of reflux.

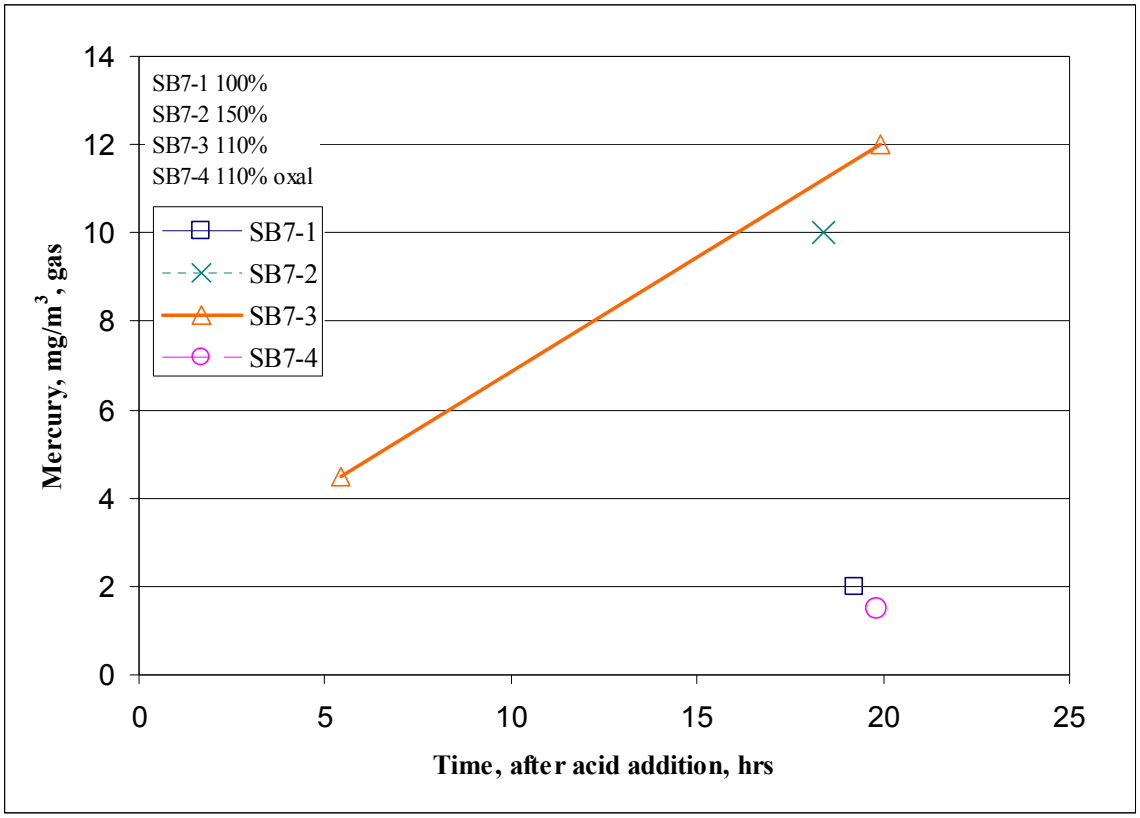

Figure 7 - Qualification Gaseous Mercury Measurements

By comparing the slurry and gaseous mercury concentrations in Figures 6 and 7, the following observations were made: a) SB7-1 had a slow decrease in the slurry and a low gas concentration, b) SB7-2 showed a substantial gas concentration late in the reflux regime despite a very sudden and substantial decrease of the slurry mercury very early in the reflux, c) SB7-3 slurry concentration slowly decreased while the gas concentration increased substantially during the same time interval, and d) SB7-4 exhibited an end-of-acid slurry mercury concentration that was a factor of ten lower than the other runs but a gas concentration roughly equal to that of the low acid run. Due to the sparseness of the gas data and to the uncertainty in the slurry mercury levels, little more can be inferred about mercury processing or chemistry.

In order to try to understand the fate of mercury in the system, a mass balance is shown in Table 19. The last column indicates that more than half of the mercury was unaccounted for in each of

the four runs. The average Hg gas concentration is listed and, taking into account the time interval and volumetric flow rate of the total off-gases, a very small mass was lost to off-gassing, several milligrams. The uncertainty of Hg gas concentration due to sparse data, Figure 7, is thus irrelevant due to the small mass loss. Nonetheless, these estimated Hg gas masses are included in the calculation of missing Hg in Table 19. It can be speculated that the "missing mercury" was likely to have been in the SRAT/SME kettle.

Table 19 - Qualification Mercury Balance

Run ID	Hg input, g	SRAT Dewater recovery, Hg (aq), g	SRAT MWWT recovery, g †	SME product recovery, g	Average [Hg] gas, mg / m^3	Total Hg recovery, g	Missing Hg %
SB7-1	12.90	0.22	4.18	0.27	2	4.67	64
SB7-2	12.90	0.01	1.61	0.16	10	1.79	86
SB7-3	12.90	0.20	3.61	0.43	8	4.25	67
SB7-4	12.90	0.12	3.01	0.49	1.5	3.62	72

† The Hg masses listed in the SRAT MWWT are from the liquid phase only because the combination of low aqueous concentrations and low overall mass of the liquid make the dissolved Hg masses very low, less than 10 mg; nonetheless, though not listed, these masses have been used in the calculation of the total recovered Hg.

More evidence that the missing mercury for SB7-2 was stuck in the kettle can be obtained by examining the mercury levels in the combined SRAT MWWT dewater condensate, Table 20.

The high acid run demonstrates:

- a relatively low level of dissolved Hg in the SRAT MWWT dewater condensate.
- a relatively lower value of undissolved mercury in the MWWT at the end of the SRAT run (Table 19)
- an abrupt and rapid decrease in SRAT slurry mercury **(**Figure 6) between the end of acid addition and the end of dewatering.

If the mercury did not end up in the off-gas system, then it is likely that it remained in the vessel.

Table 20 - Mercury Levels in Qualification Dewater Condensate

Run ID	$[Hg]_{aq}$, mg/L condensate
SB7-1	223
SB7-2	12.9
SB7-3	222
SB7-4	155

3.1.5 *Qualification Slurry Rheology*

Rheology measurements were obtained for both the SRAT products, Table 21, and SME products, Table 22. Figures 22 through 29 show the flow curves of the qualification SRAT and SME products. Because of time-dependent phenomena in some up curves, the down curves were used

to calculate the steady-state rheological model properties of the slurries. As expected the high acid qualification run, SB7-2, showed the smallest yield stress and consistency by the end of the SRAT cycle. The second thinnest SRAT product was the high oxalate run, SB7-4. The SRAT product with the highest yield stress was that of the baseline run, while the highest consistency was shown by the low acid run (though it was closely followed by the baseline run, and the difference was within the uncertainty of the measurements). SB7-4 had the highest concentration of soluble solids, perhaps due to the additional oxalate, as well as having the lowest yield stress of the three low acid runs.

Table 21 - Qualification SRAT Products Rheology

	SB7-1 Low Acid	SB7-2 High Acid	SB7-3 Baseline Acid	SB7-4 High Oxalate
Yield Stress, Pa, Down	2.9	1.4	3.3	2.2
Consistency, cP, Down	12.7	4.7	12.6	9.9
Wt % IS	16.1	14.7	14.6	14.5

The SME rheology, exhibited a somewhat different trend; this is not unusual since the addition of frit and subsequent dewatering greatly affects the rheology. The smallest yield stress still corresponds to the high acid run but the smallest consistency was found in the high oxalate run. Like the SRAT products, the SME product with the highest yield stress was that of the baseline run while the highest consistency was in the low acid run. The reasons for this are unclear.

Table 22 - Qualification SME Products Rheology

	SB7-1 Low Acid	SB7-2 High Acid	SB7-3 Baseline Acid	SB7-4 High Oxalate
Yield Stress, Pa, Down	20	8.3	24	12.0
Consistency, cP, Down	38	31	31	25
Wt % IS	41.3	39.3	39.3	39.1

The SME flow curves, given in the Appendix, were difficult to fit to the Bingham plastic model, but the values in Table 22 place the data in the approximate relative neighborhood.

3.2 Flowsheet CPC Simulations

Five runs, SB7-5 through SB7-9, were performed for the SB7 flowsheet portion of this work. Table 23 shows the acid stoichiometric factors and total acid added per liter of starting sludge.

Table 23 - Flowsheet Runs Acid Levels

Run ID - Function	Acid, mol/L	Hsu factor	KMA factor†
SB7-5 - Low acid	1.18	102%	100%
SB7-6 - High acid	1.80	155%	150%
SB7-7 - ARP-MCU	1.57	107%	110%
SB7-8 - Extended	1.33	112%	110%
SB7-9 - Baseline Acid	1.33	112%	110%

† Koopman minimum acid

3.2.1 *Flowsheet Elemental/Ion Analyses*

The following ten tables (Tables 24 through 33) show general properties, anion concentrations, and elemental concentrations of the SRAT and SME products. Figure 15, in the Appendix, shows the pH profiles of the flowsheet runs.

One noteworthy feature is that the high acid run exhibited the lowest mercury concentrations in the slurry, roughly half of some other runs; this was true for both the SRAT and SME products and for both the flowsheet and qualification (see above) runs. This behavior parallels the unusually rapid decreases of mercury concentration versus time seen in the SB6-G high acid simulant runs.[17]

Table 24 - Properties of SB7 Flowsheet SRAT Products

	SB7-5 Low Acid	SB7-6 High Acid	SB7-7 ARP-MCU	SB7-8 Extended	SB7-9 Baseline Acid
Wt% Total Solids	24.5	23.7	25.7	24.2	23.9
Wt% Insoluble Solids	15.8	14.7	15.4	15.6	14.4
Wt% Soluble Solids	8.7	9.0	10.3	8.6	9.5
Wt% Calcined	17.1	15.8	17.6	17.1	16.7
Slurry density, g/mL	1.14	1.18	1.19	1.14	1.11
Supernate density, g/mL	1.07	1.07	1.08	1.07	1.07
pH at 25°C	8.3	7.9	7.6	8.6	7.9
Wt% Hg, solids basis †	0.042	0.021	--	0.123	0.040

† The reported mercury concentrations are unlikely (see Section 3.2.4).

The next table contains the anion compositions of the dewatered condensate taken from the SRAT following formic acid addition.

Table 25 - Flowsheet SRAT Dewater Anions

	SB7-5 Low Acid	SB7-6 High Acid	SB7-7 ARP-SME Products	SB7-8 Extended	SB7-9 Baseline Acid
Nitrite, mg/L	< 100	< 100	<100	<100	<100
Nitrate, mg/L	4,360	2,430	5,410	3,620	4,500
Formate, mg/L	205	< 100	260	235	250
Sulfate, mg/L	< 100	< 100	<100	<100	<100
Chloride, mg/L	< 100	< 100	<100	<100	<100

Table 26 gives the slurry anions of the five SRAT products. The table also includes *intermediate* values of the NO_2^- ion concentration that were measured after about 75% of the SRAT reflux had elapsed (these samples were not caustic quenched, and are presumed to be lower bounds on nitrite). Oxalate was only analyzed by the IC acid strike method for the SME products, so no SRAT product oxalate data are given.

Table 26 - Flowsheet SRAT Product Anions

	SB7-5 Low Acid	SB7-6 High Acid	SB7-7 ARP-SRAT Products	SB7-8 Extended	SB7-9 Baseline Acid
Intermediate Nitrite	470	< 100	< 100 ‡	< 100	< 100
Nitrite, mg/kg	< 100	< 100	< 100	< 100	< 100
Formate, mg/kg	36,750	42,050	43,850	36,400	38,050
Nitrate, mg/kg	20,100	23,850	23,450	21,850	22,700
Sulfate, mg/kg	1,250	1,170	2,290	1,310	1,160
Chloride, mg/kg	310	250	490	320	310

‡ During the ARP-MCU run, the intermediate value of NO_2^- concentration was measured after about 75% of the total SRAT post-dewater interval (i.e., MCU boiling + SRAT reflux) had elapsed or about half-way through the reflux process.

The intermediate nitrite concentration measured for the low acid (100% Koopman minimum acid) run was of interest; Table 26 shows that this value is 470 mg/kg slurry, which indicates a low, but detectable, concentration. The nitrite was consumed by the end of the SRAT cycle. Thus, the Koopman minimum acid equation again (see qualification case above) seems to have predicted the amount of acid necessary to destroy nitrite reasonably accurately. All five SRAT products show complete destruction of nitrite. The anion chemistry, Table 27, shows no unusual behavior.

Table 27 - Flowsheet SRAT Anion Reactions

	SB7-5 Low Acid	SB7-6 High Acid	SB7-7 ARP-MCU	SB7-8 Extended	SB7-9 Baseline Acid
Nitrite Loss %	100	100	100	100	100
Net Nitrite-to-Nitrate %	11	-17	9	8	14
Formate Loss %	25	43	19	34	28
Formate Lost, g	37.5	92.5	28.2	54.8	45.7

Formate loss increased with increasing acid stoichiometry. Formate loss also increased with increasing processing time. Nitrite-to-nitrate conversion tended to decrease with increasing acid stoichiometry and increasing processing time, but these results are not statistically significant.

SRAT product calcined elemental data are given in Table 28.

Table 28 - Calcined Elemental Composition, wt%, of Flowsheet SRAT Products (1100 °C)

Element	SB7-5 Low Acid	SB7-6 High Acid	SB7-7 ARP-MCU	SB7-8 Extended	SB7-9 Baseline Acid
Al	15.7	15.5	13.8	15.5	15.4
Ba	0.109	0.111	0.112	0.119	0.117
Ca	0.845	0.845	0.873	0.794	0.794
Ce	0.162	0.168	0.147	0.184	0.184
Cr	0.070	0.070	0.075	0.080	0.078
Cu	0.074	0.082	0.072	0.039	0.046
Fe	20.3	20.0	17.8	19.6	19.7
K	0.113	0.126	0.117	0.119	0.113
La	0.081	0.081	0.072	0.089	0.089
Li	< 0.1	< 0.1	< 0.1	< 0.1	< 0.1
Mg	0.408	0.409	0.490	0.453	0.444
Mn	4.97	4.89	4.45	5.05	5.00
Na	14.3	14.6	16.7	14.7	15.0
Ni	3.39	3.28	2.77	3.27	3.30
Pb	0.023	0.025	0.030	0.030	0.022
Rh	< 0.1	< 0.1	< 0.1	< 0.1	< 0.1
Ru	< 0.1	< 0.1	< 0.1	< 0.1	< 0.1
S	0.354	0.351	0.419	0.383	0.340
Si	1.79	1.76	1.57	1.74	1.72
Ti	0.027	0.030	2.96	0.030	0.030
Zn	0.063	0.061	0.068	0.064	0.063
Zr	0.253	0.263	0.261	0.269	0.268

SB7-7 elemental values should not match the other four runs, since the ARP slurry solids have a different composition from the SB7-A simulant solids. SB7-7 contained mono sodium titanate, MST, which is evident in the titanium and sodium elemental data. Elemental supernate compositions for these five SRAT products are given in Table 29.

Table 29 - Elemental Composition of Flowsheet SRAT Product Supernates

Element	SB7-5 Low Acid mg/L	SB7-6 High Acid mg/L	SB7-7 ARP-MCU mg/L	SB7-8 Extended mg/L	SB7-9 Baseline Acid, mg/L
Al	0.946	0.867	0.949	0.435	0.382
B	1.32	1.36	1.13	6.2	10.8
Ca	17.2	47.1	8.71	5.87	28.2
Ce	0.168	1.55	< 0.1	0.45	< 0.1
Cr	< 0.1	< 0.1	< 0.1	< 0.1	< 0.1
Cu	0.262	0.670	0.18	< 0.1	< 0.1
Fe	< 1	< 1	< 1	< 1	< 1
K	403	366	743	487	442
Li	< 10	< 10	< 10	< 10	< 10
Mg	70.1	368	235	21.5	166
Mn	285	3,570	905	70.0	1,040
Ni	0.170	6.75	7.02	< 0.1	0.397
Rh	< 1	1	< 1	< 1	< 1
Ru	< 1	2	< 1	< 1	< 1
S	731	684	1039	639	619
Si	23.4	27.8	23.2	60.0	14.4
Sn	0.351	3.31	N/A	N/A	N/A
Ti	0.164	0.170	< 0.1	< 0.1	< 0.1
Zn	< 0.1	< 0.1	< 0.1	< 0.1	< 0.1
Zr	< 0.1	< 0.1	< 0.1	< 0.1	< 0.1

The elemental supernate data are similar to that for the four qualification runs in that they show very little dissolution of the insoluble sludge solids. One exception was Mn in the high acid run, which was significantly dissolved.

The next tables give similar property data for the five SME products.

Table 30 - Properties of Flowsheet SME Products

	SB7-5 Low Acid	SB7-6 High Acid	SB7-7 ARP-MCU	SB7-8 Extended	SB7-9 Baseline
Wt% Total Solids	47.9	47.9	52.8	48.0	47.7
Wt% Insoluble Solids	39.7	39.5	41.8	40.3	38.7
Wt% Soluble Solids	8.2	8.4	11.1	7.7	9.0
Wt% Calcined	41.2	40.7	45.1	41.7	40.9
Slurry density, g/mL	1.32	1.40	1.47	1.40	1.38
Supernate density, g/mL	1.09	1.10	1.12	1.09	1.09
pH at 25°C	8.1	7.4	7.4	8.2	7.6
Wt% Hg, total solids	0.109	0.010	--	0.028	0.021

Table 31 - Flowsheet SME Product Anions

	SB7-5 Low Acid	SB7-6 High Acid	SB7-7 ARP-MCU	SB7-8 Extended	SB7-9 Baseline Acid
Nitrite, mg/kg	< 100	< 100	< 100	< 100	< 100
Nitrate, mg/kg	19,550	21,050	21,500	18,400	19,600
Formate, mg/kg	35,400	39,350	43,800	33,250	35,450
Sulfate, mg/kg	1,020	1,130	2,205	1,100	1,065
Chloride, mg/kg	235	225	466	282	271
Oxalate, mg/kg	8,300	9,000	11,000	8,700	8,500

Material balances were used to determine losses of the various anions. For oxalate, the loss is the combined SRAT/SME cycle loss, while the other losses are for the SME cycle only. REDOX values ($Fe^{2+}/\Sigma Fe$) were predicted for these SME products. Measured values are discussed in a separate memo.[20] SME anion reaction results are given in Table 32. Loss percentages less than 10% absolute magnitude (20% in the case of oxalate) are not statistically distinguishable from zero.

Table 32 - Flowsheet SME Anion Reactions and REDOX

	SB7-5 Low Acid	SB7-6 High Acid	SB7-7 ARP-MCU	SB7-8 Extended	SB7-9 Baseline Acid
Nitrate Loss, %	-4	8	11	7	5
Formate Loss, %	8	4	4	5	3
Formate Lost, g	7.7	8.7	11.7	6.9	5.3
Oxalate Loss, %	13	4	6	4	4
Predicted REDOX	0.18	0.20	0.21	0.18	0.19

The SME elemental data for both the calcined and supernate phases are given below in Table 33 and Table 34 respectively. The waste loading targets for four of the five flowsheet runs were 36.0%. The post-run mass balance waste loading values varied from 35.2% to 36.0%. Frit 418 was used.

Table 33 - Calcined Elemental Composition, wt%, of Flowsheet SME Products (1100 °C)

Element	SB7-5 Low Acid	SB7-6 High Acid	SB7-7 ARP-MCU	SB7-8 Extended	SB7-9 Baseline
Al	5.92	5.93	5.36	6.11	5.93
B	1.42	1.38	1.42	1.42	1.43
Ba	0.039	0.042	0.042	0.041	0.042
Ca	0.351	0.366	0.372	0.377	0.353
Ce	0.060	0.059	0.051	0.061	0.062
Cr	0.037	0.044	0.031	0.028	0.046
Cu	0.027	0.020	0.038	0.025	0.034
Fe	7.39	7.27	6.74	7.31	7.07
K	0.074	0.089	0.119	0.090	0.086
La	0.027	0.030	0.025	0.029	0.030
Li	2.21	2.22	2.18	< 0.1	2.22
Mg	0.162	0.163	0.196	0.171	0.172
Mn	1.81	1.76	1.61	1.81	1.73
Na	9.28	9.22	9.91	9.73	9.58
Ni	1.18	1.17	1.03	1.20	1.17
Pb	0.013	0.012	0.012	0.012	0.012
Rh	< 0.1	< 0.1	< 0.1	< 0.1	< 0.1
Ru	< 0.1	< 0.1	< 0.1	< 0.1	< 0.1
S	0.106	0.119	0.138	0.110	0.103
Si	23.9	23.9	22.2	23.4	22.5
Ti	0.052	0.055	1.15	0.058	0.056
Zn	0.021	0.035	0.025	0.023	0.024
Zr	0.173	0.190	0.182	0.186	0.189

Table 34 - Elemental Composition of Flowsheet SME Product Supernates

Element	SB7-5 Low Acid mg/L	SB7-6 High Acid mg/L	SB7-7 ARP-MCU mg/L	SB7-8 Extended mg/L	SB7-9 Baseline Acid, mg/L
Al	1.02	1.04	0.934	0.351	0.340
B	6.38	24.3	36.3	6.20	10.8
Ca	42.0	71.9	32.7	29.6	49.1
Ce	0.731	2.64	0.45	< 0.1	< 0.1
Cr	< 0.1	< 0.1	< 0.1	< 0.1	< 0.1
Cu	0.556	0.793	0.222	0.225	0.168
Fe	< 1	< 1	18.2	< 1	< 1
K	507	482	1,120	633	585
Li	223	228	< 10	< 10	< 10
Mg	178	506	469	89.8	299
Mn	1,460	5,830	3,310	410	2,760
Ni	1.48	19.0	37.7	0.243	4.23
Rh	< 1	1	< 1	< 1	< 1
Ru	< 1	5	< 1	< 1	< 1
S	960	940	1,5530	880	860
Si	15.5	41.9	33.4	24.4	15.3
Sn	1.57	5.73	N/A	N/A	N/A
Ti	0.186	0.167	< 0.1	< 0.1	< 0.1
Zn	< 0.1	< 0.1	< 0.1	< 0.1	< 0.1
Zr	< 0.1	< 0.1	< 0.1	< 0.1	< 0.1

Mn solubility seemed to increase in SB7-7 and SB7-9 relative to the SRAT product. The SB7-6 oxalate concentration remained high. These points seem to indicate that the oxalate is not what is controlling Mn solubility variations in these data. The majority of the other initially insoluble elements remained out of the supernate phase. The presence of detectable supernate Rh and Ru is consistent with the catalytic activity of the high acid run, SB7-6.

3.2.2 *Flowsheet GC Results*

The flowsheet runs peak hydrogen generation rates did not exceed the design basis limits of 0.65 and 0.223 lb/h for the SRAT and SME cycles, respectively, as was also the case with the qualification data. Table 35 shows the peak gas generation rates as measured by the GC during the SRAT cycles and converted to full-scale DWPF generation rates. More detailed GC time profile data are shown in Figures 8, 9, and 10. Since these figures are congested and do not show the SME data clearly, the SME cycle data are graphed separately and given in the Appendix; see Figures 19-21. Hydrogen production was greatest in the highest acid run, as expected. The next highest producers of hydrogen were the baseline and extended runs, both at 110% acid level. The ARP-MCU SB7-7 run exhibited reduced hydrogen production, perhaps due to additional oxalate consumption of acid. This is similar to the behavior exhibited by the high oxalate run, SB7-4.

Table 35 - Maximum SRAT Gas Generation Rates

Gas	SB7-5 Low Acid	SB7-6 High Acid	SB7-7 ARP-MCU	SB7-8 Extended	SB7-9 Baseline
H_2, lb/h	0.005	0.31	0.02	0.06	0.06
N_2O, lb/h	15.4	30.2	13.8	15.5	24.6
CO_2, lb/h	540	629	571	305	613

The CO_2 generation rate typically peaked during TIC destruction with the rate approximately dependent on the acid addition rate at the time. Since the acid addition rate in the extended run, SB7-8, was about half that of the other runs, the rate of CO_2 generation was also reduced significantly.

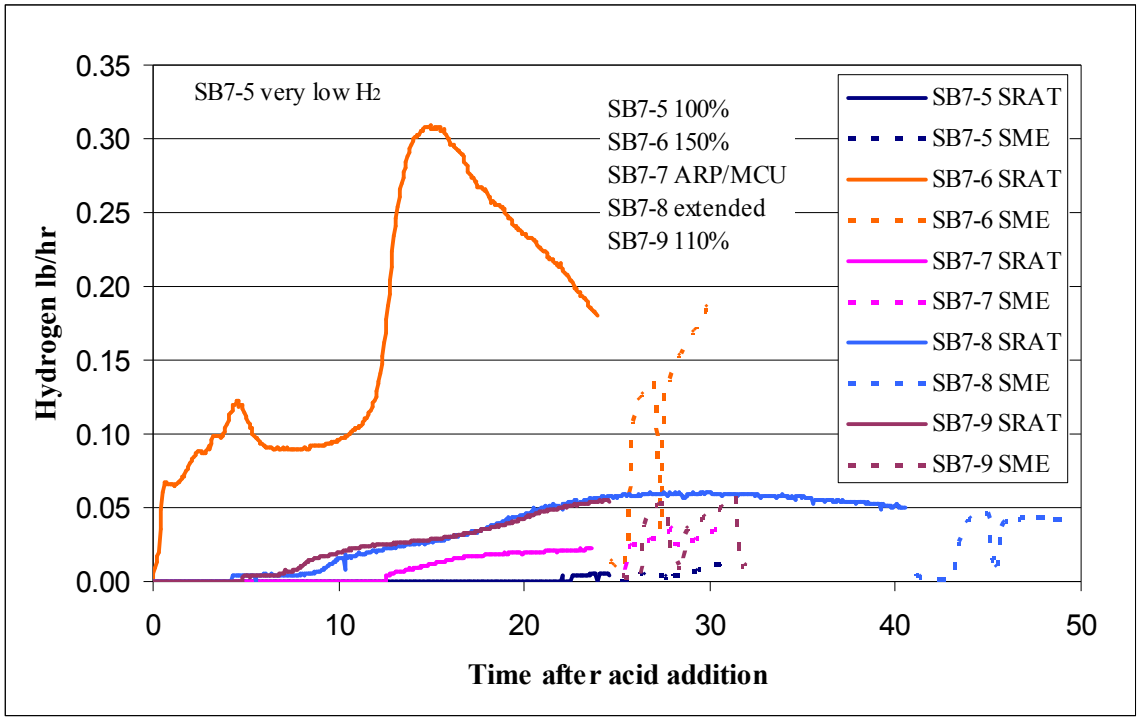

Figure 8 - Flowsheet SRAT/SME Hydrogen Profiles

Both CO_2 and N_2O production were greater in the high acid run, SB7-6 in Figure 9 and Figure 10, following acid addition. The secondary humps between about 12 and 17 hours after the end of acid addition coincide for CO_2 and H_2, but not for N_2O.

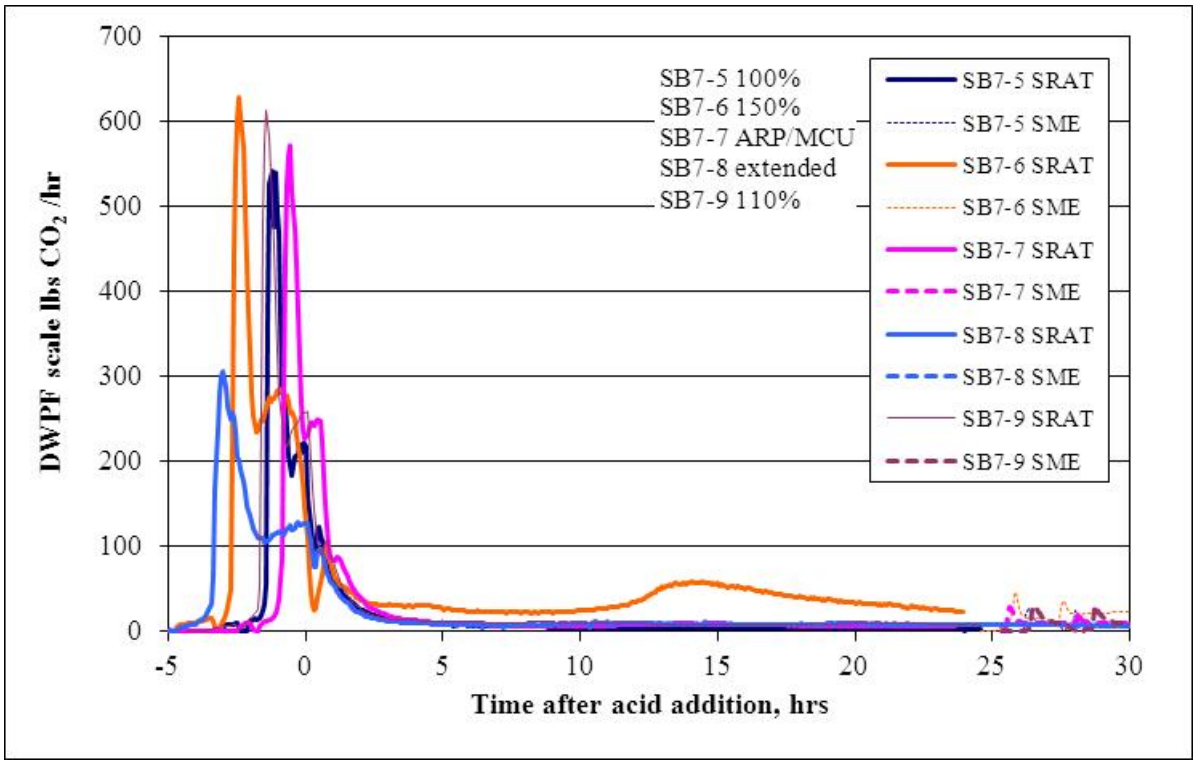

Figure 9 - Flowsheet SRAT/SME CO_2 Profiles

SB7-6 saw production of 113 g of CO_2 in the SRAT compared to 48 g in SB7-5 and 64 g in SB7-9. All three include TIC destruction. In addition the results generally tracked the formate losses in these three runs (92 g in SB7-6, 37 g in SB7-5, and 46 g in SB7-9). About 20 g of CO_2 was expected from TIC destruction. Any CO_2 from antifoam oxidation was not detectable against the background of other sources.

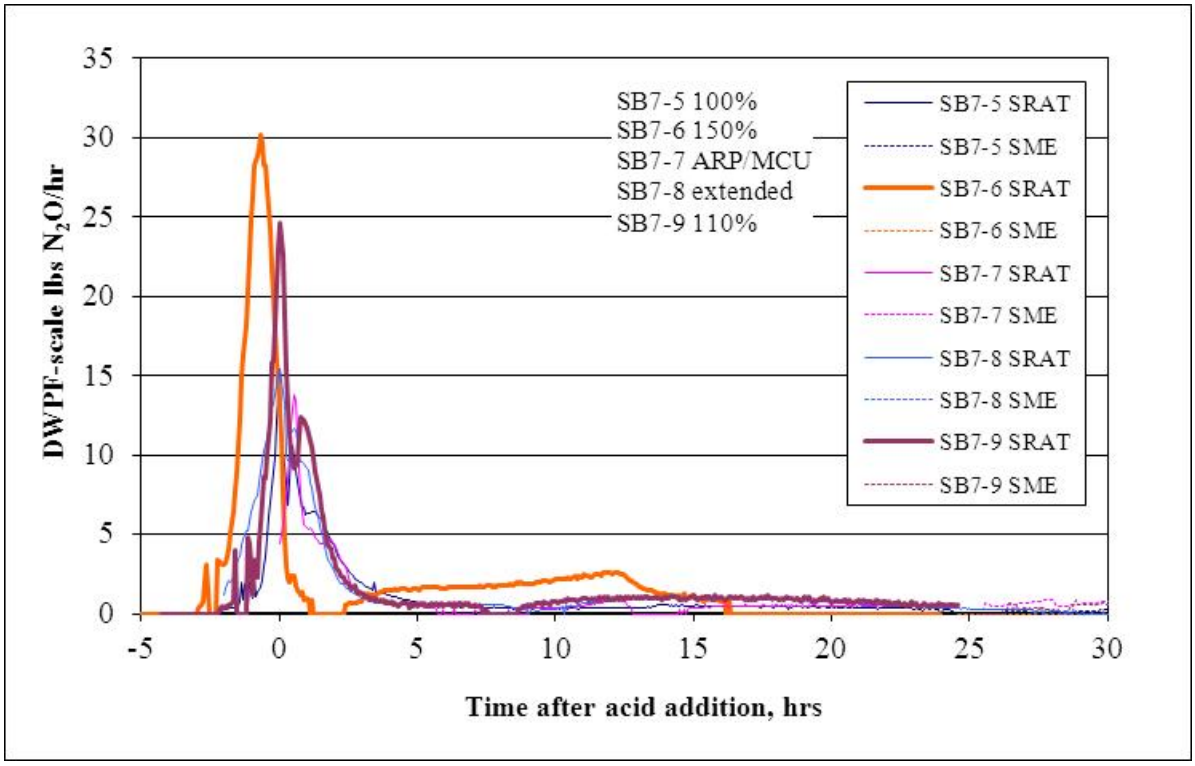

Figure 10 - Flowsheet SRAT/SME N_2O Profiles

The most N_2O was produced in the high acid run, SB7-6 (4.1 g versus <3.6 g in the others). This run produced N_2O during nitrite destruction during formic acid addition, than proceeded to produce significant additional N_2O during reflux. The second episode was likely associated with the reaction sequence leading to ammonium ion formation. The least N_2O was produced in the ARP-MCU run, SB7-7 (1.7 g versus >2.2 g in the others). The combined feed of the ARP-MCU run contained only 29.6 g of nitrite compared to 34.6 g in the other four runs. This difference probably accounts for the lower N_2O production. The two runs at 110% acid and SB7-A feed both produced about 3.2-3.6 g of N_2O, which was intermediate between the high (4.1 g) and low (2.2 g) acid values.

Maximum SME cycle gas generation rates are given in Table 36. Hydrogen reached 87% of the DWPF limit in the high acid stoichiometry run.

Table 36 - Maximum SME Gas Generation Rates

Gas	SB7-5 Low Acid	SB7-6 High Acid	SB7-7 ARP-MCU	SB7-8 Extended	SB7-9 Baseline
H_2, lb/h	0.012	0.195	0.039	0.046	0.059
N_2O, lb/h	0.4	0.4	0.9	0.2	0.8
CO_2, lb/h	26	46	28	42	31

3.2.3 *Flowsheet Ammonia/Ammonium Results*

The concentrations of the ammonia in the ammonia scrubber liquid and of ammonia gas at the outlet of the SRAT condenser are shown in Figure 11. The low acid and ARP-MCU runs did not exhibit detectable production of ammonia or ammonium; this behavior is similar to the behavior of the qualification low acid and high oxalate runs. In contrast, the flowsheet high acid, extended, and baseline runs did exhibit ammonia and ammonium generation. This was similar to the high acid and baseline qualification runs. The onset of ammonia and ammonium generation for SB7 simulant was similar to that seen in the previous SB6 study[17]: as pH levels rose above neutral, ammonium and ammonia were produced; see the pH-time profiles in the Appendix, Figure 15.

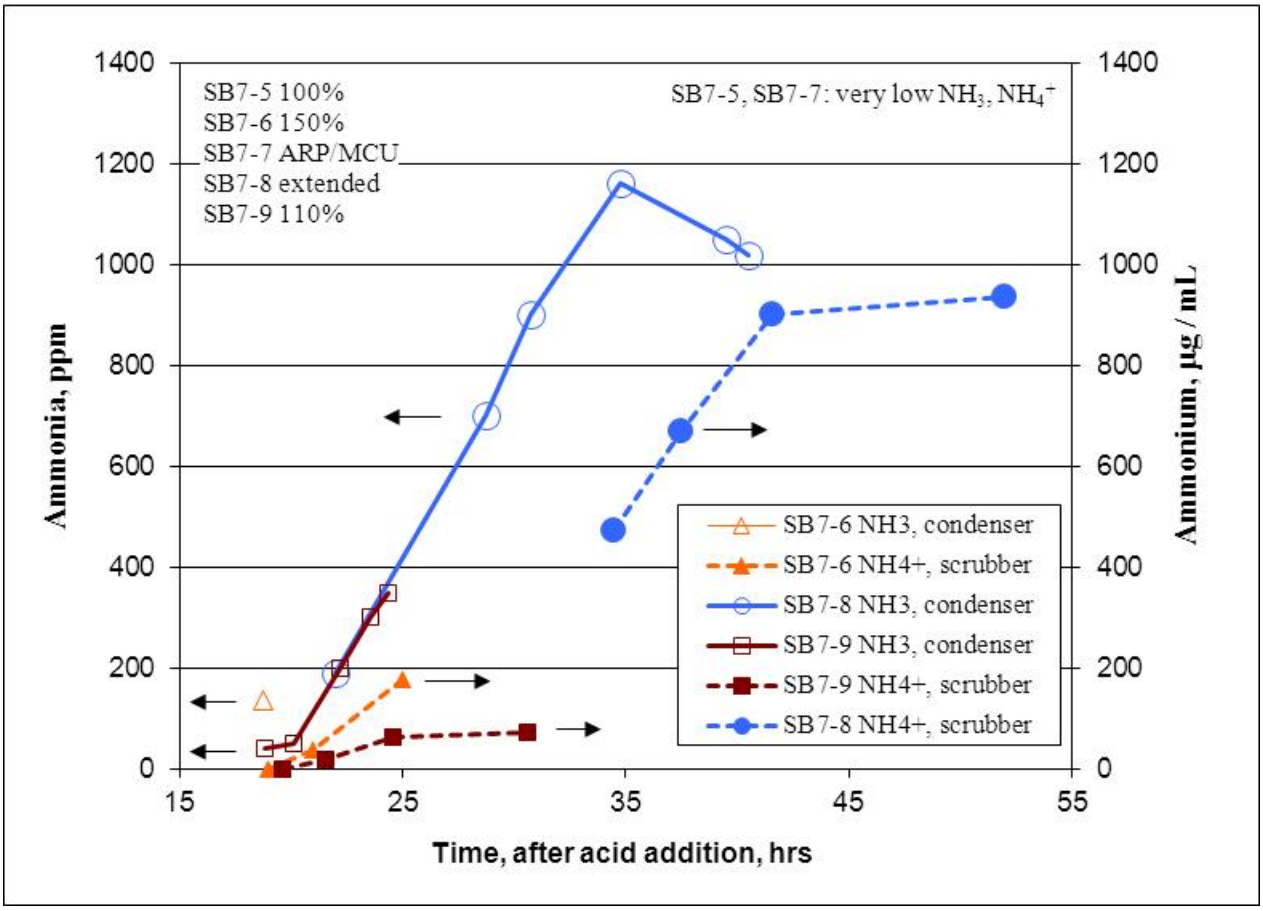

Figure 11 - Flowsheet SRAT Ammonia and Ammonium Concentrations

3.2.4 *Flowsheet Mercury Results*

The concentration of slurried mercury was measured in the SRAT/SME vessel and in the gas phase at the outlet of the SRAT condenser; the MWWT was also used to collect Hg. Mercury concentrations in the SRAT and SME product slurries are tabulated; see Table 37. There are no values listed for SB7-7 ARP-MCU mercury concentrations because the measured values were several times greater than what was added; see Figure 12 and the following discussion. Mercury

sample preparation is such that all sample mass is consumed, so suspect results cannot be checked by performing a second sample preparation and re-analyzing.

Table 37 - Mercury Composition in Flowsheet SRAT/SME Product Slurries

	SB7-5 Low Acid	SB7-6 High Acid	SB7-7 ARP-SME Products	SB7-8 Extended	SB7-9 Baseline
SRAT, wt% Hg, dried solids	0.042	0.021	--	0.123	0.040
SME, wt% Hg, dried solids	0.109	0.010	--	0.028	0.021

Figure 12 shows the Hg time profile of all five flowsheet slurries. Note that the first values at the end of acid addition refer to a slurry before dewatering. A given concentration at the end of acid addition corresponds to more mercury mass than the same concentration following dewatering. As mentioned above, the high acid run, SB7-6, shows a sudden drop in mercury concentration, consistent with SB6 high acid run behavior.[17]

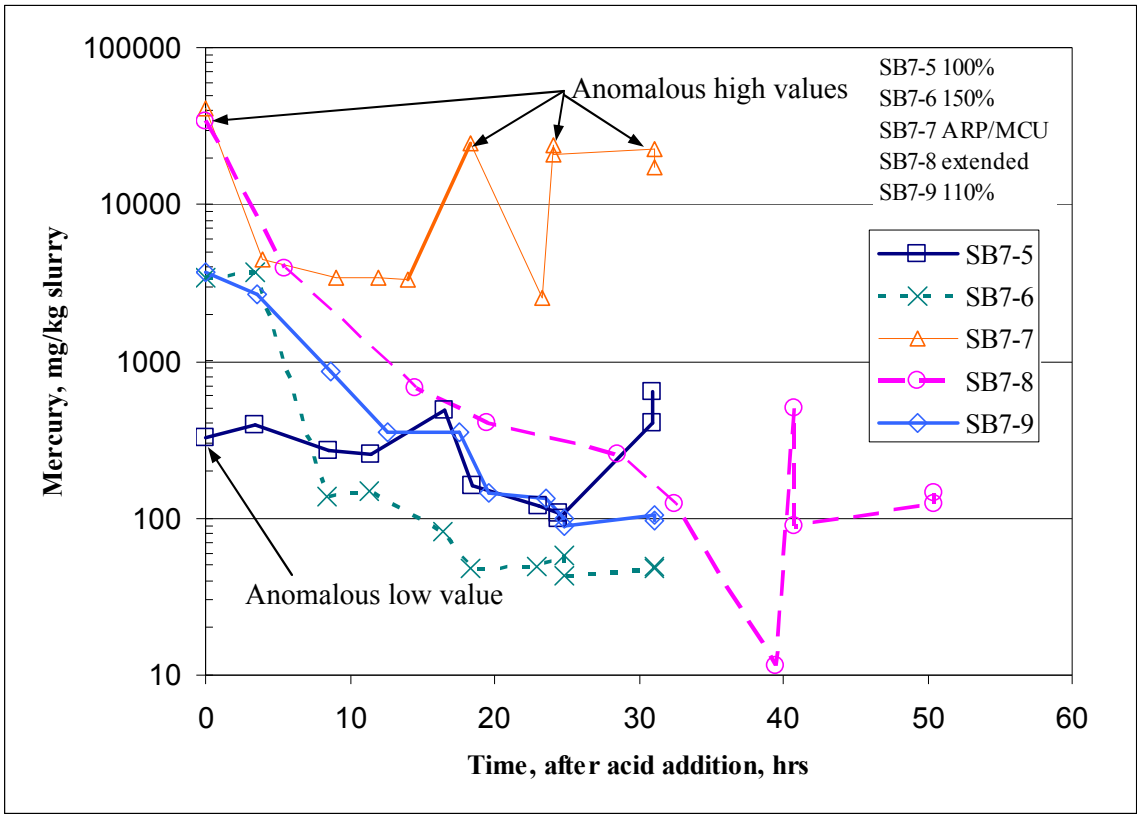

Figure 12 - Flowsheet Slurry Mercury Measurements

There is an anomalously low value series of mercury concentrations in the SB7-5 low acid case data. The qualification high oxalate run exhibited similar behavior with, a values that were also ten times lower than expected. By contrast, the ARP-MCU run exhibited high slurry concentrations that were several times greater than the amount of Hg that was trimmed into the

system. The reasons for this are presently unknown, but it is likely the result of sampling a disproportionate volume of agglomerated drops of elemental mercury with the slurry.

Mercury gas measurements are shown in Figure 13. There is nothing unusual to be seen in these sparse data other than that the low concentrations indicate minimal non-condensed mercury. It is obvious, however, that the high acid run produced a greater concentration of mercury in the gas phase than would be expected given the low slurry concentration at that time (~19 hours into reflux). The extended run also produced higher gaseous concentrations of Hg.

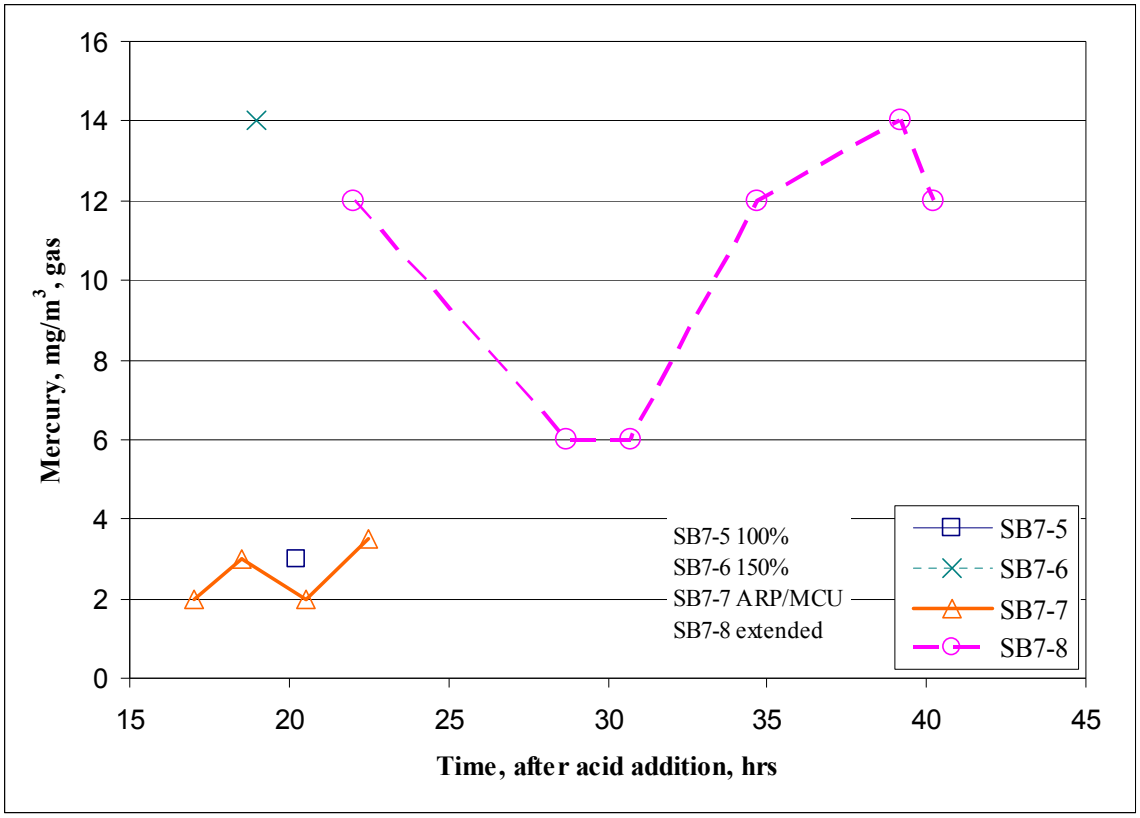

Figure 13 - Flowsheet Gaseous Mercury Measurements

In order to attempt to understand the fate of mercury in the system, a mass balance is shown in Table 38. The last column indicates that more than half of the mercury introduced to the SRAT was unaccounted for in each of the five the runs that had the necessary data. The average Hg gas concentration is listed and, taking into account the time interval and volumetric flow rate of the total off-gases, a very small mass of order several milligrams could be lost to off-gassing. The uncertainty of Hg gas concentration due to somewhat sparse data, Figure 13, is thus irrelevant due to the small mass loss. Nonetheless, these estimated Hg gas masses are included in the calculation of missing Hg in Table 38. There are missing data: a) the aqueous and liquid Hg masses in the SRAT MWWT of SB7-8 and SB7-9 were not measured, the samples were not saved, and thus the data are unavailable and b) the mercury concentration (both replicated measurements) in the SME product of the SB7-7 ARP-MCU run are about an order of magnitude greater than is possible; the values suggest about 54.2 g which is greater than the total amount of Hg trimmed in, 14.31 g.

Table 38 - Flowsheet Mercury Balance

Run ID	Hg input, g	SRAT Dewater recovery, Hg (aq), g	SRAT MWWT recovery g †	SME MWWT recovery, g	SME product recovery, g	Average [Hg] gas, mg / m^3	Total Hg recovery g	Missing Hg %
SB7-5	14.78	0.22	4.72	0	1.23	3	6.17	58
SB7-6	14.78	0.01	2.42	0	0.12	14	2.55	83
SB7-7	14.31	0.02	4.86	0.80	--	3	5.68	> 60
SB7-8	14.78	0.20	N/A	N/A	0.29	10	--	--
SB7-9	14.78	0.20	N/A	N/A	0.20	--	--	--

† The Hg masses listed in the SRAT MWWT are from the liquid phase only, because the combination of low aqueous concentrations and low overall mass of the liquid make the dissolved Hg masses very low, less than 10 mg; nonetheless, though not listed, these masses have been used in the calculation of the total recovered Hg. The water and mercury from the SRAT MWWT of SB7-8 and SB7-9 were not saved and thus the aqueous and solid Hg mass data are unavailable.

These flowsheet runs, like the qualification runs, exhibit "missing mercury"; greater than half is unaccounted for. It is likely that the missing mercury was present in the apparatus but not sampled. Two possible mechanisms are: a) the matter in the kettle is very heterogeneous and the mercury, present as small, dense agglomerates, was unlikely to be sampled and b) the mercury became stuck in a film on the inner walls of the apparatus, primarily the kettle. Based on the data available, loss of mercury by off-gassing is negligible. Subsequent observations support mercury accumulation on the vessel wall, probably at the bottom of the SRAT, in beads that are too large to suspend or break down into smaller droplets.

More evidence that the missing mercury for SB7-6 was stuck in the kettle can be obtained by examining the mercury levels in the combined SRAT dewater-MWWT condensate**,** Table 39. The high acid run demonstrates: a) a relatively low level of dissolved Hg in the SRAT MWWT dewater condensate, b) a relatively lower value of undissolved mercury in the MWWT at the end of the SRAT run (Table 38), and c) a very sudden and overwhelming decrease in SRAT slurry mercury (Figure 12) between the end of acid addition and the end of dewatering. If the mercury did not end up in the off-gas system, then it is likely that it remained in the vessel. This phenomenon was also observed during the qualification and SB6 work.

Table 39 - Mercury Levels in Flowsheet Dewater Condensate

Run ID	$[Hg]_{aq}$, mg/L condensate
SB7-5	251
SB7-6	7.28
SB7-7	8.05
SB7-8	232
SB7-9	229

Moreover, the SRP-MCU run, SB7-7, while exhibiting a comparable recovery in the SRAT MWWT at the end of reflux, yields a low value of aqueous dewater condensate in the MWWT (this is very similar to that of the high acid run). It is unclear why this occurred.

3.2.5 *Flowsheet Rheology*

Rheology measurements were obtained for both the SRAT products, Table 40, and SME products, Table 41. Figures 30 through 39 in the Appendix show the flow curves of the flowsheet SRAT and SME products. Because of time-dependent behavior in some of the up curves, the down curves were utilized to determine the steady-state rheological properties. As expected the high acid flowsheet run, SB7-6, shows the smallest yield stress and consistency by the end of the SRAT cycle. The second thinnest SRAT product by yield stress is the baseline run, SB7-9. The thickest SRAT products correspond to either the low acid or ARP-MCU run. These runs had the highest insoluble solids wt%.

Table 40 - Flowsheet SRAT Product Rheology

	SB7-5 Low Acid	SB7-6 High Acid	SB7-7 ARP-SRAT Products	SB7-8 Extended	SB7-9 Baseline
Yield Stress, Pa, Down	4.7	1.1	4.1	7.1	3.3
Consistency, cP, Down	16	5.5	14	8.1	14
Wt % insoluble solids	15.8	14.7	15.4	15.6	14.4

Because the slurries were concentrated to different levels of insoluble solids in the SME process, Table 41, and since the rheology is very sensitive to this value, the trends have changed relative to those of the SRAT products. Here, the smallest yield stress still corresponds to the high acid run but the rest of the data suggest a more complex dependence on processing conditions.

Table 41 - Flowsheet SME Product Rheology

	SB7-5 Low Acid	SB7-6 High Acid	SB7-7 ARP-SME Products	SB7-8 Extended	SB7-9 Baseline
Yield Stress, Pa, Down	35	12	23	37	28
Consistency, cP, Down	52	24	50	33	46
Wt % insoluble solids	40	40	42	40	39

The flowsheet SME products were better behaved rheologically than the qualification set as shown in the Appendix. Fits to the Bingham plastic model equation were more accurate.

4.0 Conclusions

DWPF Chemical Process Cell (CPC) flowsheet testing was completed with qualification and flowsheet simulants for Sludge Batch 7. The goals were to determine reasonable operating conditions and detect any possible difficulties or issues regarding the processing of the blend SB6/SB7 (i.e., flowsheet or Tank 40) and the "pure" SB7 (i.e., qualification or Tank 51) sludge. The testing covered the domain from 100 to 150% of the Koopman minimum acid equation or about 102 to 155% using the current DWPF-Hsu acid equation.

Nitrite ion concentrations were reduced to 760 and <100 mg/kg slurry in the qualification and flowsheet 100% acid (KMA) SRAT products. These data indicate that the Koopman equation accurately predicted the acid needs of the qualification simulant and those of the flowsheet simulant to a lesser degree. However, even though the flowsheet value could mean an overestimate of the needed acid for nitrite destruction, an intermediate value of nitrite concentration, measured after 75% of the SRAT reflux had elapsed, yielded a small value of 472 mg/kg. This indicates that while the acid need of the flowsheet simulant was overestimated by KMA, this prediction was still reasonably close to the true minimum acid demand.

The high acid runs produced the highest hydrogen gas generation, but both the flowsheet and qualification cases never exceeded about 85% of the maximum allowable hydrogen generation rates in the SRAT and SME cycles. The acid processing window for SB7 blended feed is approximately 102 to 155% Hsu. It is recommended that 110% KMA or 112% Hsu be used for SB7 processing.

There were few problems with SB7 simulant processing. A very small amount of foaming was detected around the agitator shafts during SB7-2 (qualification, high acid) and SB7-5 (flowsheet, low acid) but this foaming was not considered problematic. Also there were no instances of ammonia scrubber column flooding. Based on the simulants, the SRAT or SME products, both qualification and flowsheet, should not cause significant issues with mixing or transferring, since the rheology was within DWPF limits. The SME product data indicate that all of the runs satisfied the 36% waste loading target. The performance of an extended run at the prototypical DWPF conditions (1 gallon per minute acid addition and 3,000 lb/h of steam) did not cause any significant problems or changes in gas generation or rheology. Mercury stripping was not satisfactory, and the reasons remain unclear. As with SB6, the high acid runs appeared to undergo a very sudden drop in slurried mercury; it is possible that this is due to some complexation of mercury with noble metals in the SRAT vessel or gravity settling.

The addition of simulated Actinide Removal Process (ARP) and Modular Caustic Side Solvent Extraction Unit (MCU) streams to the SRAT cycle did not influence the recommended acid stoichiometry. The increase of oxalate concentration in the qualification study did not cause any lab-scale processing difficulties but decreases in both hydrogen production and mercury stripping were observed. This observation is relevant as part of the SB7 originates from Tank 7 which, after the enhanced chemical cleaning, contains a high concentration of oxalate.

The acid strike oxalate method appears to be able to quantify both sludge and SME product oxalate for SB7 when the proper dilution range and instrument are used. The method is less accurate than weighted dilution formate and nitrate analysis at the present time. The data obtained indicated that nearly all of the simulant oxalate was water soluble prior to SRAT processing. This may not be the case for the material removed from Tanks 5 and 6 using oxalic

acid cleaning that make up part of SB7. A significant quantity of calcium and/or magnesium oxalate in the starting feed could invalidate the current Koopman minimum acid equation which assumes they are 75% basic (hydroxide or carbonate). The seven SME products all showed only small changes in oxalate mass which were indistinguishable from the initial oxalate within the uncertainty of the oxalate IC analysis.

There are enduring questions about the fate of mercury. The mercury balance has not been fully closed and as much as 58% to 86% of the mercury is unaccounted for. It is likely that the mercury either stuck to the inner surfaces of the apparatus, mostly in the SRAT/SME kettle, or it is possible that the mercury was reduced to the elemental form and remained as part of a heterogeneous, globular component in the SME product; this second possibility would also make sampling difficult because of the small likelihood of capturing a piece of isolated globules of mercury in the slurry, even under agitation. Unlike the Phase III SB6 high acid runs,[15] there was no visible deposition of mercury or mercury amalgams on the agitator shaft or blades.

There was a significant amount of ammonium and ammonia generated as the pH rose above neutral during the SRAT cycles, as was the case for SB6.[15, 17] Secondary peak production of hydrogen, CO_2, and N_2O in the high acid runs of both flowsheet and qualification simulant seemed to coincide, suggesting that a common reactant was involved in the production of these gases. The production of ammonia and ammonium is likely related to these precursor gases and there is evidence from the SB6 Phase III study that a possible mechanism for producing ammonia would require a catalyst of either Ru or a mercury amalgam;[15] there is no evidence here that would argue against the proposed reaction model.

5.0 Recommendations and Path Forward

It is recommended that DWPF process SB7 at the following acid stoichiometry: 110% KMA or about 112% Hsu. If the need should arise, small steps of 5% increases in acid stoichiometry up to about 155% Hsu could be used in the search for optimal processing. Experimental redox measurements of the flowsheet SME products will be published in a separate report where they can be compared to the 90% confidence intervals about the current model.

There are unanswered questions regarding the fate of mercury. A follow-up study to this work is being performed and published in a separate report. It involves a detailed analysis of the mercury balance from SRAT/SME cycles, including a detailed examination of the remaining material and apparatus coatings from the flowsheet runs of SB7. Another investigation could involve the characterization of mercury or amalgam species in the SME products from this work; this is similar to the aforementioned Phase III SB6 study which revealed mercury amalgams coating the shaft and agitator blades and free mercury in the SME product sludge. It is possible that these amalgams could be resistant to steam stripping. More information is needed regarding the speciation and fate of the “missing mercury” in SB7.

6.0 References

1. Bricker, J.M., *Technical Task Request for Sludge Batch 7 Flowsheet Studies*, HLW-DWPF-TTR-2010-0012, Savannah River Site, Aiken, SC 29808, 2010.
2. Fernandez, A.I., *Task Technical and Quality Assurance Plan for Sludge Batch 7 Simulant Flowsheet Studies*, SRNL-RP-2010-0071, Savannah River National Laboratory, Aiken, SC 29808, 2010.
3. Ketusky, E.T., *Re-investigating the Process Impacts from Oxalic Acid High Level Waste Tank Cleaning*, WSRC-STI-2008-00036, Westinghouse Savannah River Company, Aiken, SC 29808, 2008.
4. Adu-Wusu, K., et al., *Waste Tank Heel Chemical Cleaning Summary*, WSRC-TR-2003-00401, Westinghouse Savannah River Company, Aiken, SC 29808, 2003.
5. Davis, N., et al., *Enhanced Chemical Cleaning: A New Process for Chemically Cleaning Savannah River Waste Tanks-9100*, WSRC-STI-2008-00035, Washington Savannah River Company, Aiken, SC 29808, 2009.
6. Poirier, M.R., et al., *Removing Sludge Heels from Savannah River Site Waste Tanks by Oxalic Acid Dissolution-9120*, SRNL-SETI-2008-00466, Savannah River National Laboratory, Aiken, SC 29808, 2008.
7. Stone, M.E., *Lab-Scale CPC Equipment Set-Up*, SRNL-PSE-2006-00074, Savannah River National Laboratory, Aiken, SC 29808, 2010.
8. Koopman, D.C., *A Comparison of Rheology Data for Radioactive and Simulant Savannah River Site Waste*, WSRC-TR-2004-00044, Savannah River National Laboratory, Aiken, SC 29808, 2004.
9. Newell, J.D., *Simulant Development for Sludge Batch 6*, SRNL-STI-2010-00219, Savannah River National Laboratory, Aiken, SC 29808, 2010.
10. Pareizs, J.M. and D.R. Click, *Chemical Characterization Results of the SRNL-Washed Tank 51 Sludge Batch 7 Qualification Sample*, SRNL-L3100-2010-00252, Savannah River National Laboratory, Aiken, SC 29808, 2010.
11. Fellinger, T.L., et al., *Macrobatch 3 Acceptance Evaluation - data from the Shielded Cells Demonstration of Defense Waste Processing Facility's Feed Preparation Cycles for Macrobatch 3 (Sludge Batch 2)*, WSRC-RP-2001-00971, Washington Savannah River Company, Aiken, SC 29808, 2001.
12. Pareizs, J.M., et al., *Sludge Batch 3 Qualification in the SRTC Shielded Cells*, WSRC-TR-2004-00050, Washington Savannah River Technology Company, Aiken, SC 29808, 2004.
13. Pareizs, J.M., *Demonstration of the DWPF Flowsheet in the SRNL Shielded Cells in Support of Sludge Batch 4 Qualification*, WSRC-STI-2007-00053, Savannah River National Laboratory, Aiken, SC 29808, 2007.
14. Pareizs, J.M., et al., *Sludge Washing and Demonstration of the DWPF Flowsheet in the SRNL Shielded Cells for Sludge Batch 5 Qualification*, SRNS-STI-2008-00111, Savannah River National Laboratory, Aiken, SC 29808, 2008.
15. Koopman, D.C., *Sludge Batch 6/Tank 40 Simulant Chemical Process Cell Simulations*, SRNL-STI-2010-00212, Savannah River National Laboratory, Aiken, SC 29808, 2010
16. Koopman, D.C., D.R. Best, and B.R. Pickenheim, *SRAT Chemistry and Acid Consumption During Simulated DWPF Melter Feed Preparation*, WSRC-STI-2008-00131, Washington Savannah River Company, Aiken, SC 29808, 2008.
17. Fernandez, A.I., *Sludge Batch 6 Supplemental SRAT Runs: Effects of Yield Stress and Cycle Time Increase*, SRNL-STI-2010-00307, Savannah River National Laboratory, Aiken, SC 29808, 2010.

18. Coleman, C.J., *Method to Determine Oxalate in High-Level Sludge by Ion Chromatography*, WSRC-TR-2002-00497, Westinghouse Savannah River Company, Aiken, SC 29808, 2002.
19. Herman, C.C., et al., *Sludge Batch 3 Simulant Flowsheet Studies: Final Phase SRAT/SME Results*, WSRC-TR-2003-00422, Westinghouse Savannah River Company, Aiken, SC 29808, 2003.
20. Newell, J. D., Defense Waste Processing Facility (DWPF) Sludge Batch 7 (SB7) REDOX Evaluation, SRNL-L3100-2011-00062, SRNL, Aiken, SC, 29808.

Appendix A
Additional Data

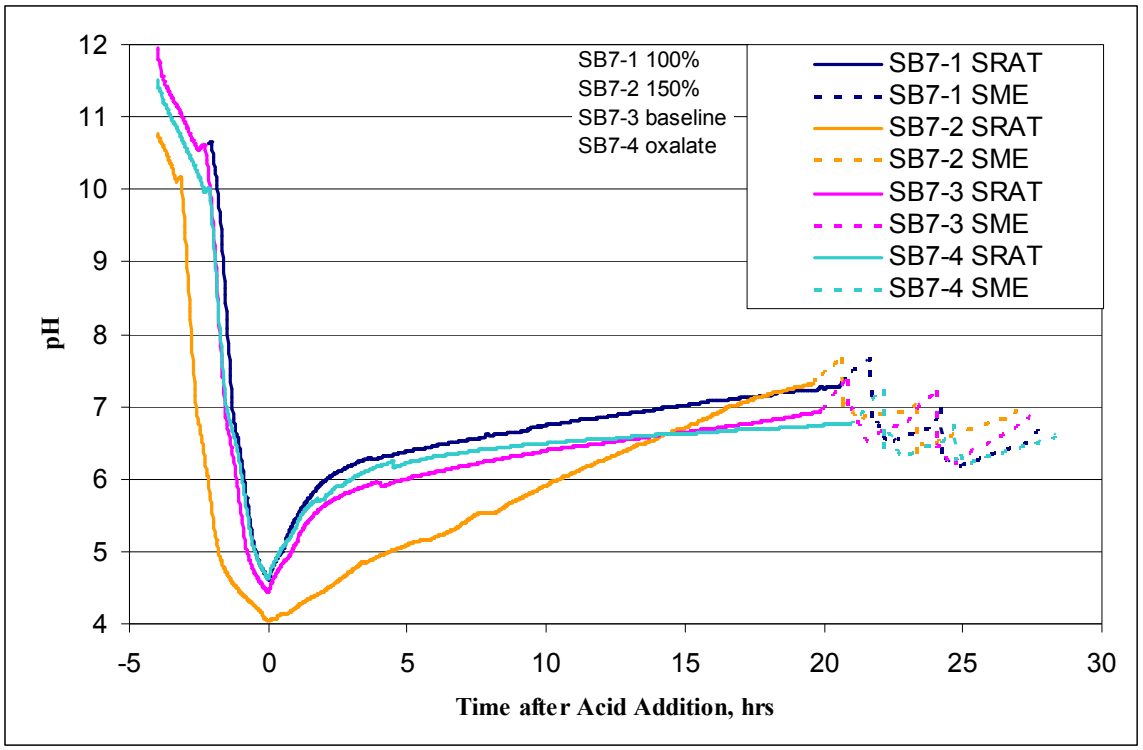

Figure 14 - Qualification pH Time Profiles

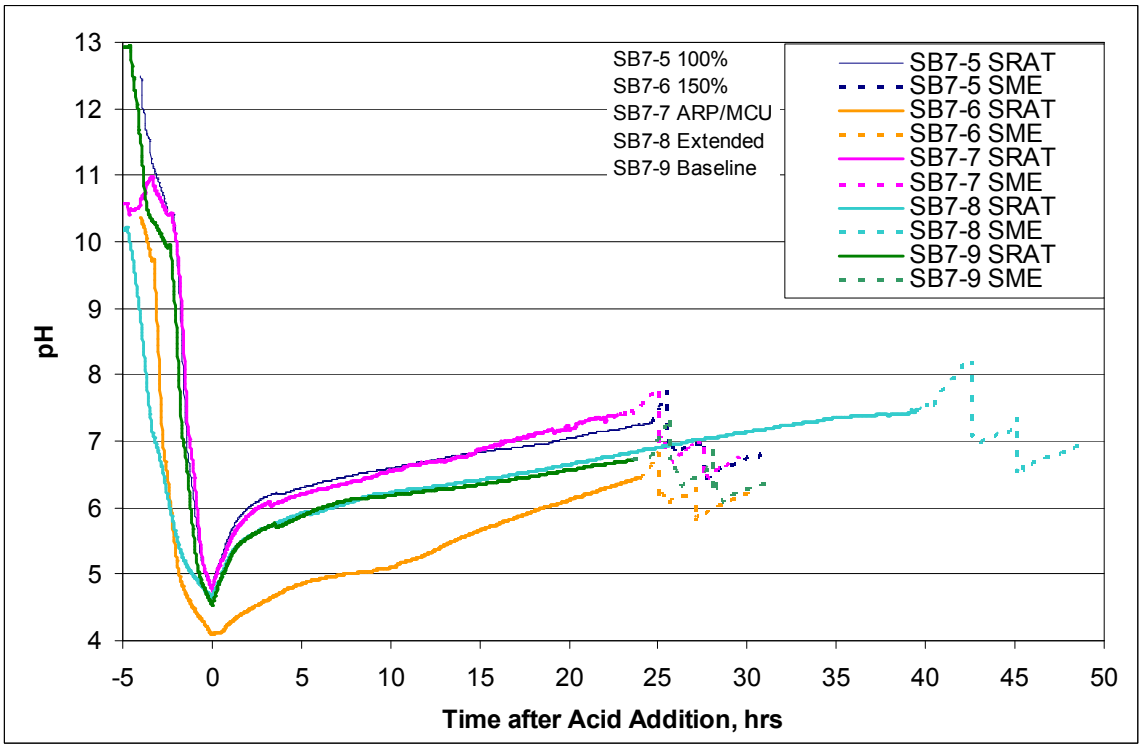

Figure 15 - Flowsheet pH Time Profiles

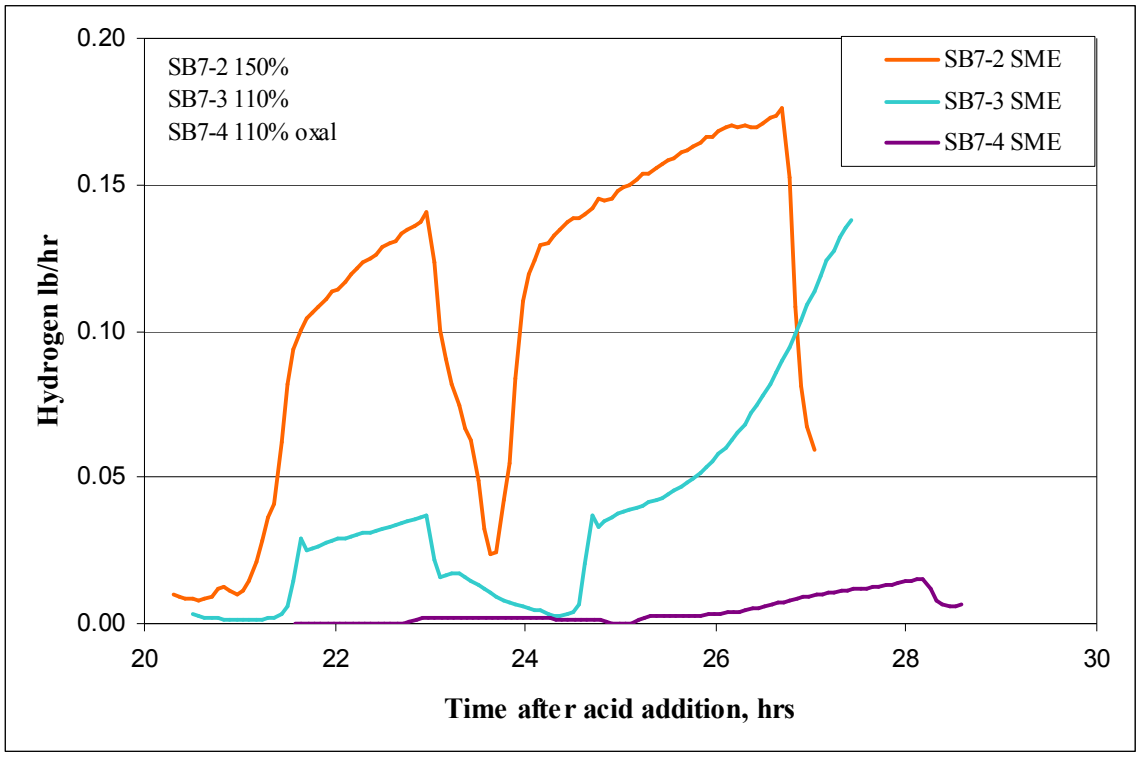

Figure 16 - Qualification SME Hydrogen Generation

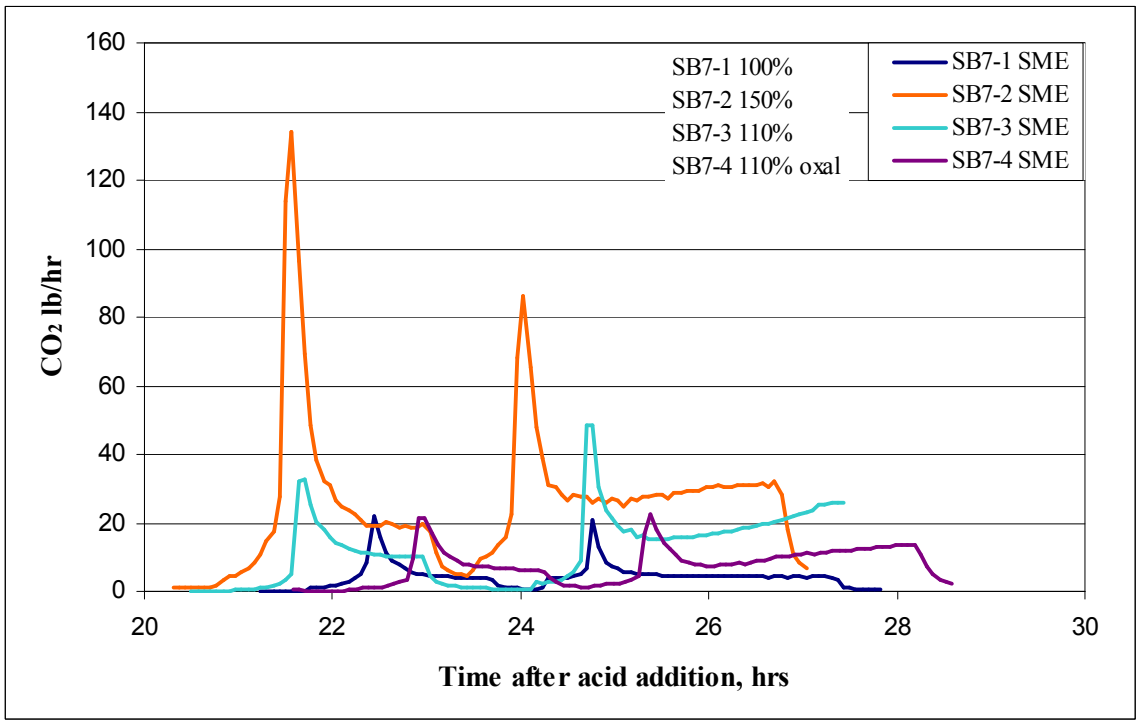

Figure 17 - Qualification SME CO_2 Generation

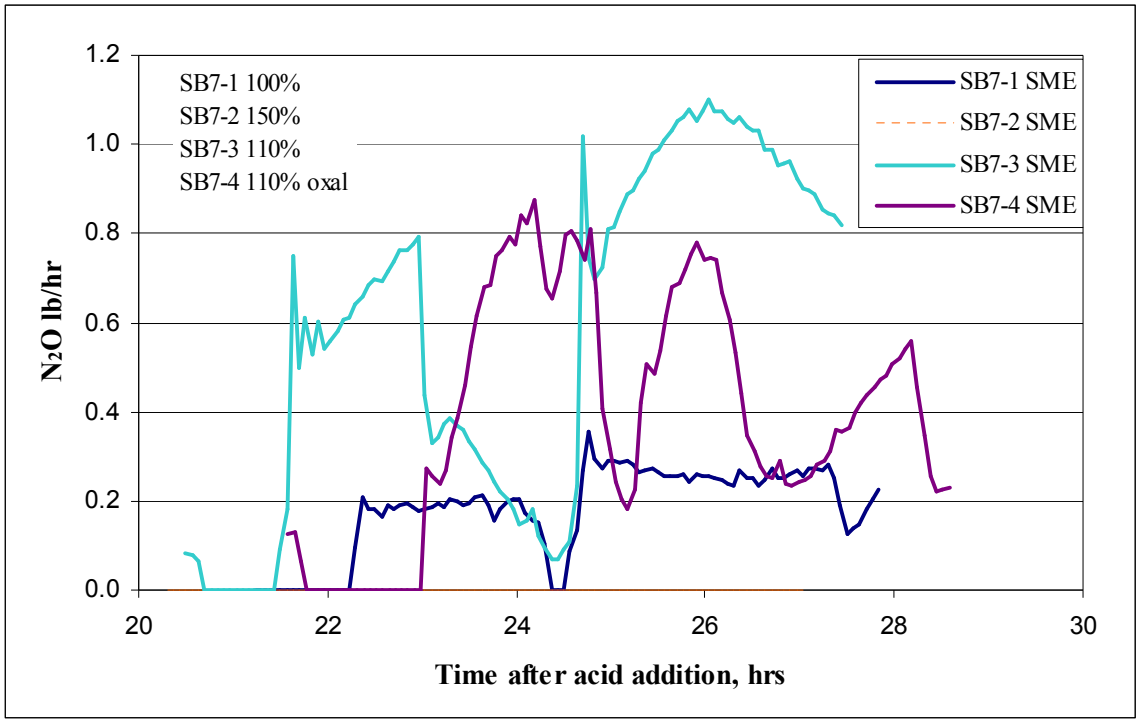

Figure 18 - Qualification SME N_2O Generation

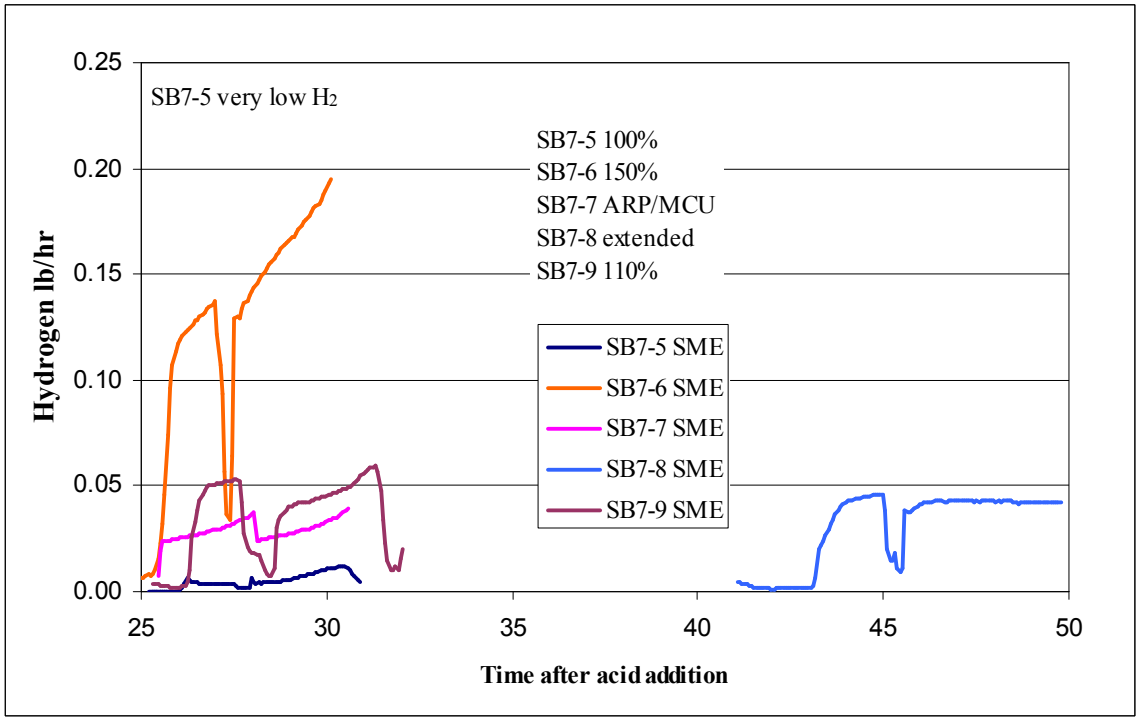

Figure 19 - Flowsheet SME Hydrogen Generation

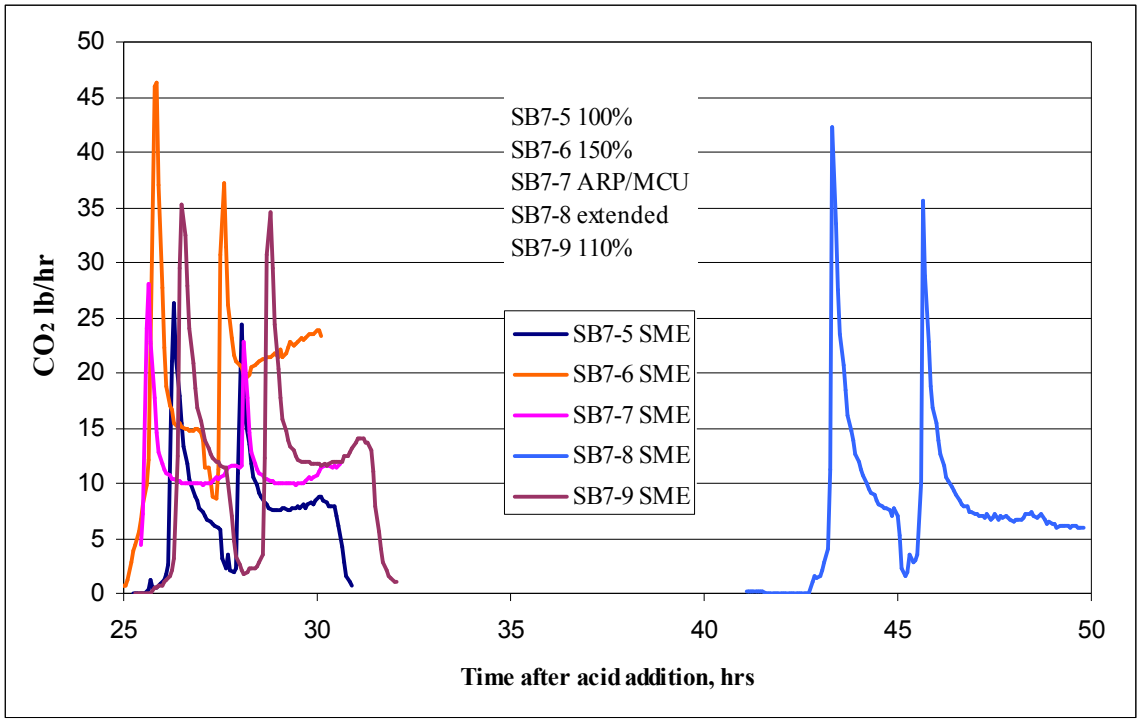

Figure 20 - Flowsheet SME CO_2 Generation

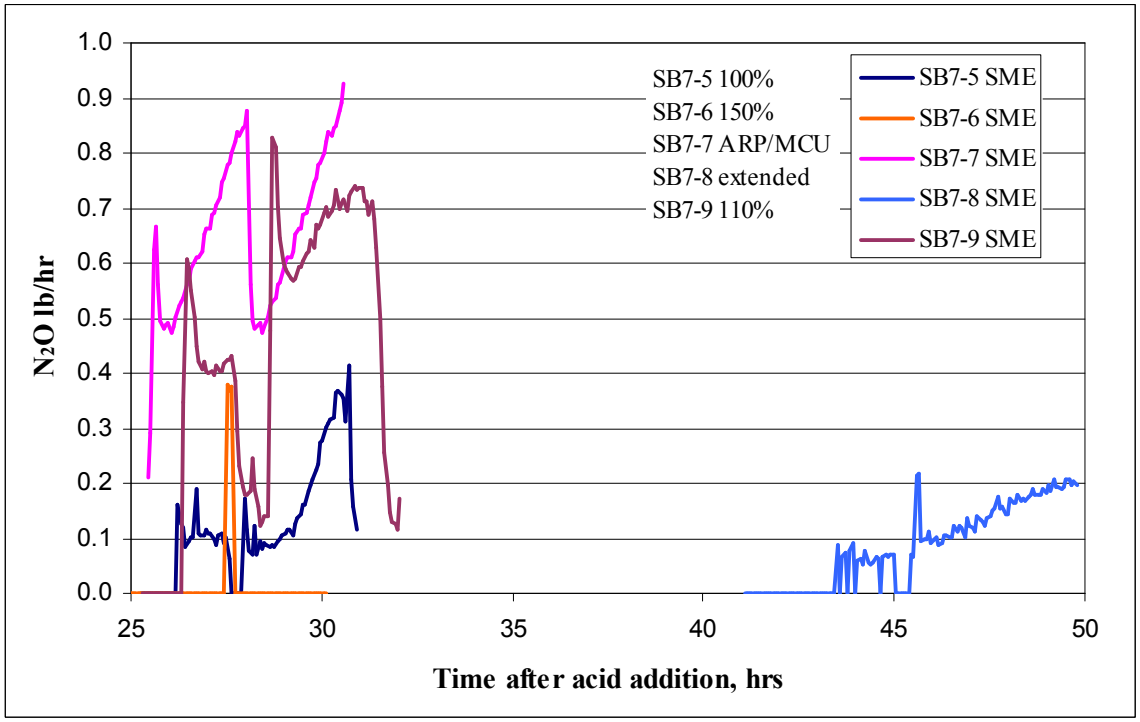

Figure 21 - Flowsheet SME N_2O Generation

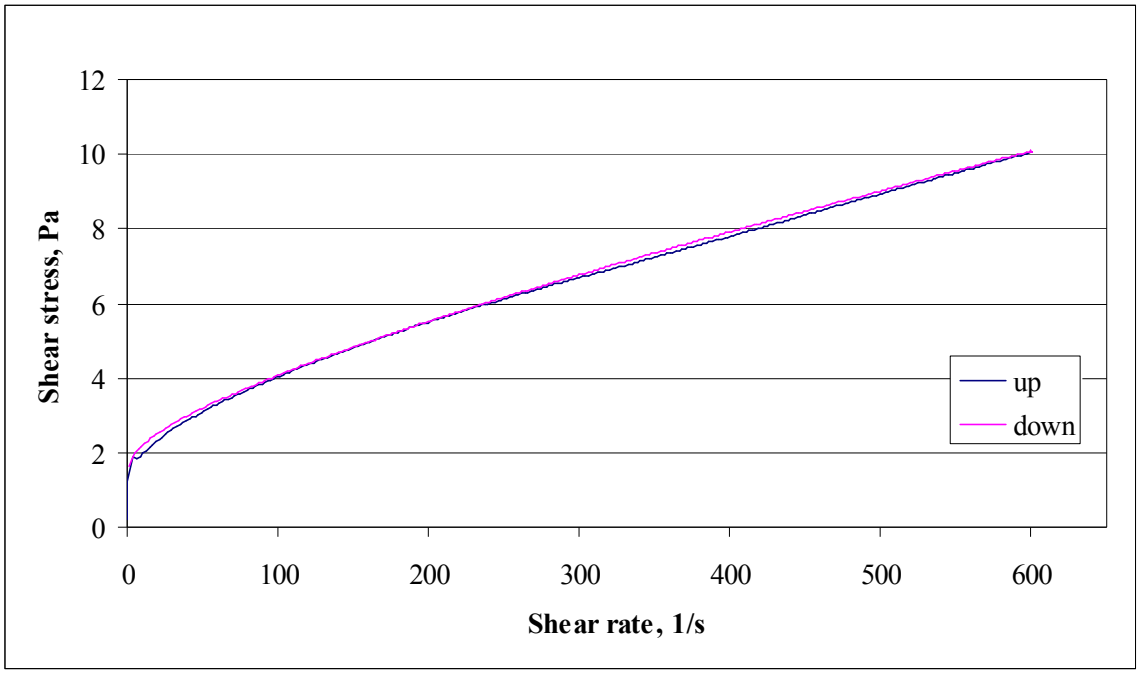

Figure 22 - SB7-1 SRAT Rheology Flow Curve

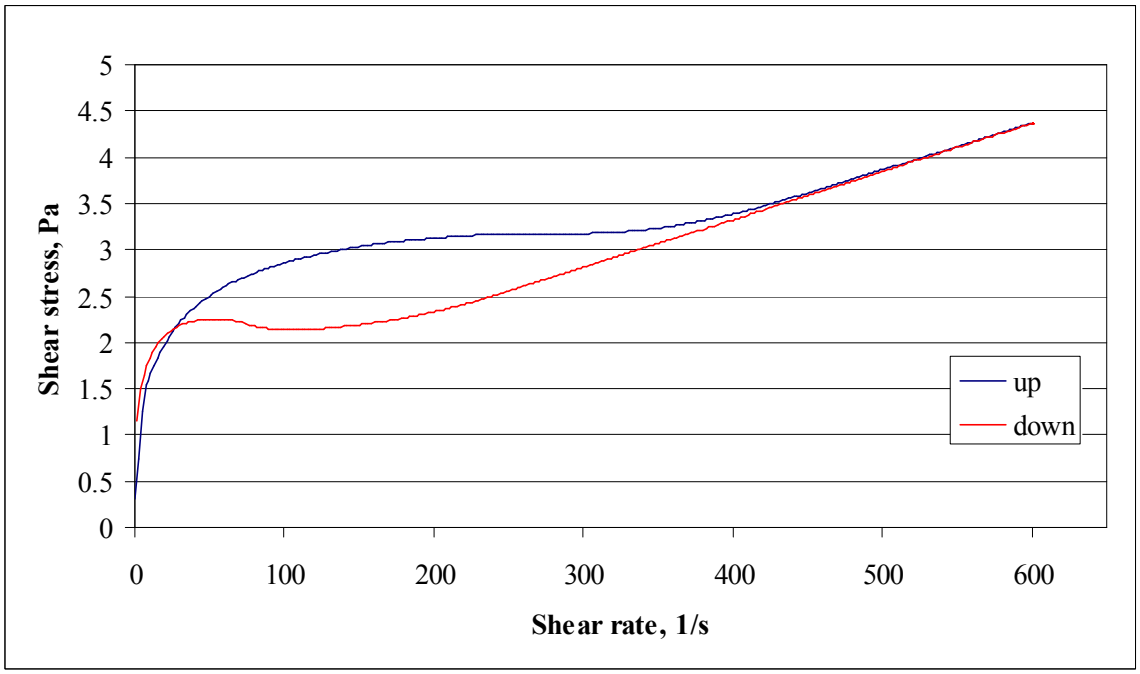

Figure 23 - SB7-2 SRAT Rheology Flow Curve

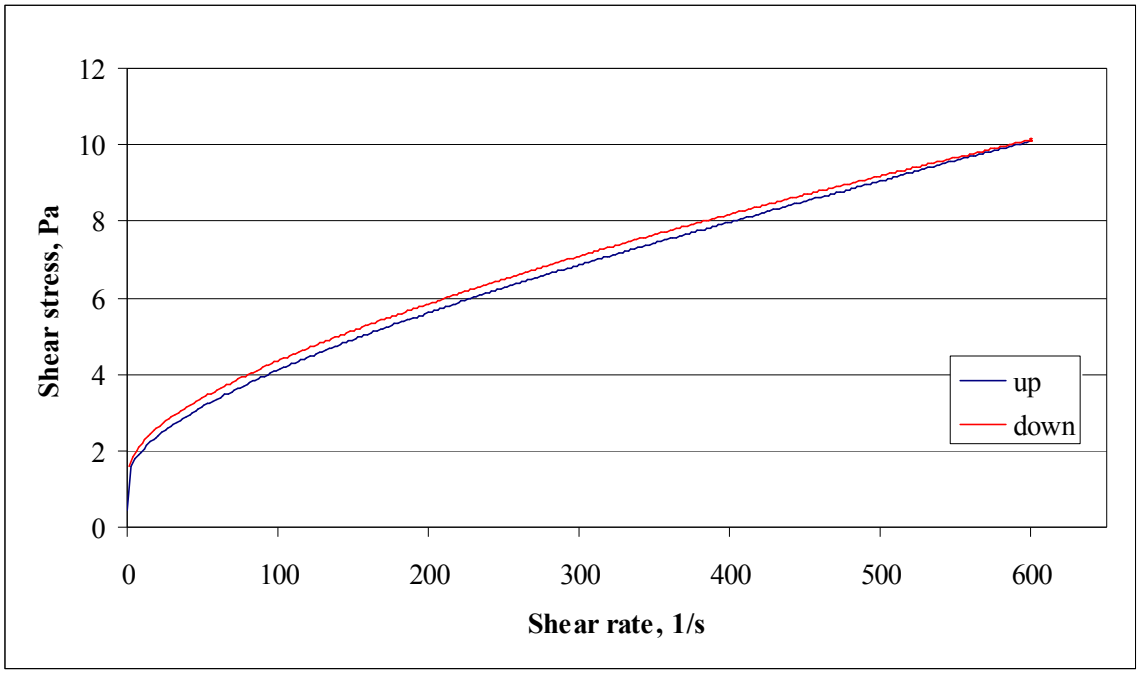

Figure 24 - SB7-3 SRAT Rheology Flow Curve

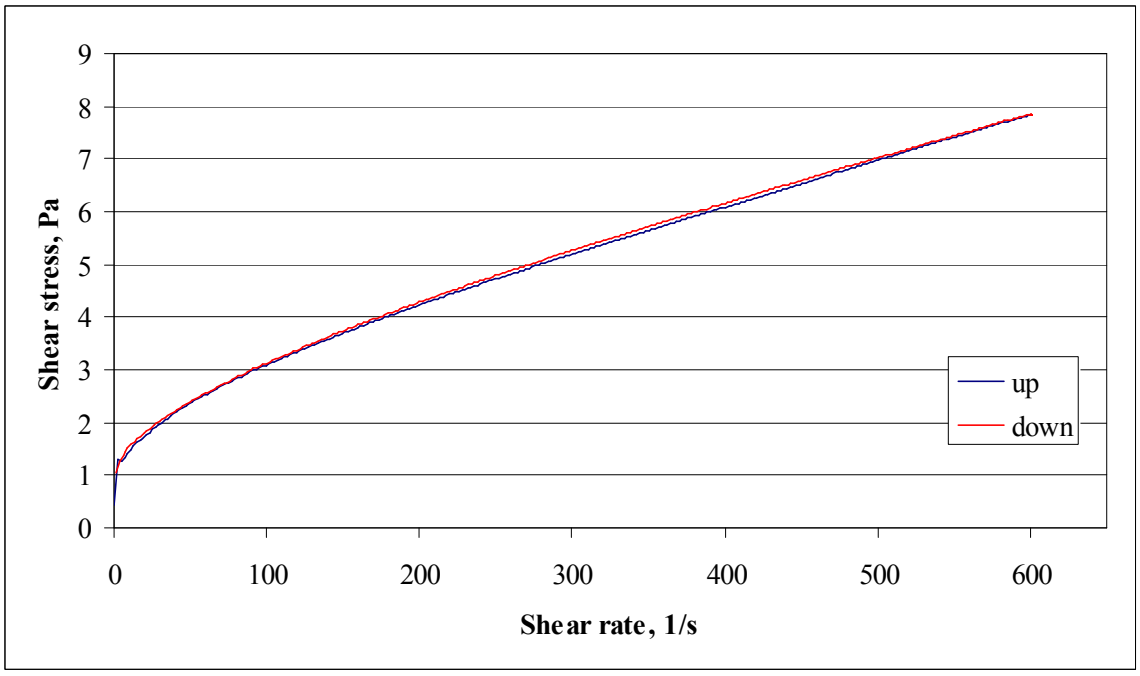

Figure 25 - SB7-4 SRAT Rheology Flow Curve

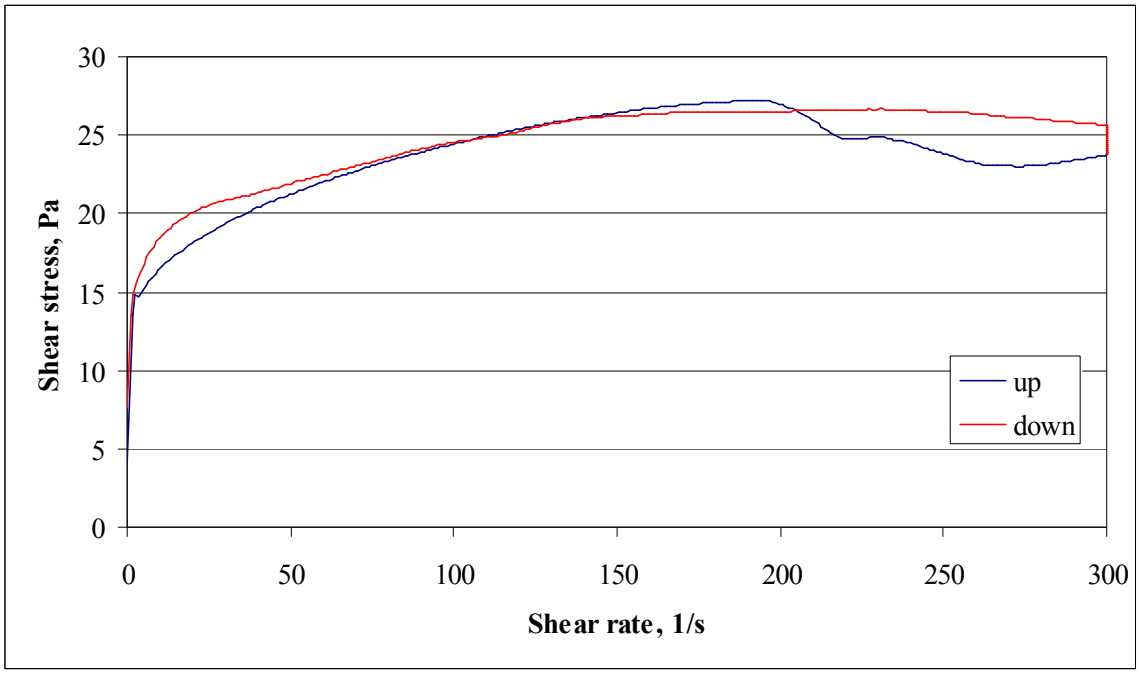

Figure 26 - SB7-1 SME Rheology Flow Curve

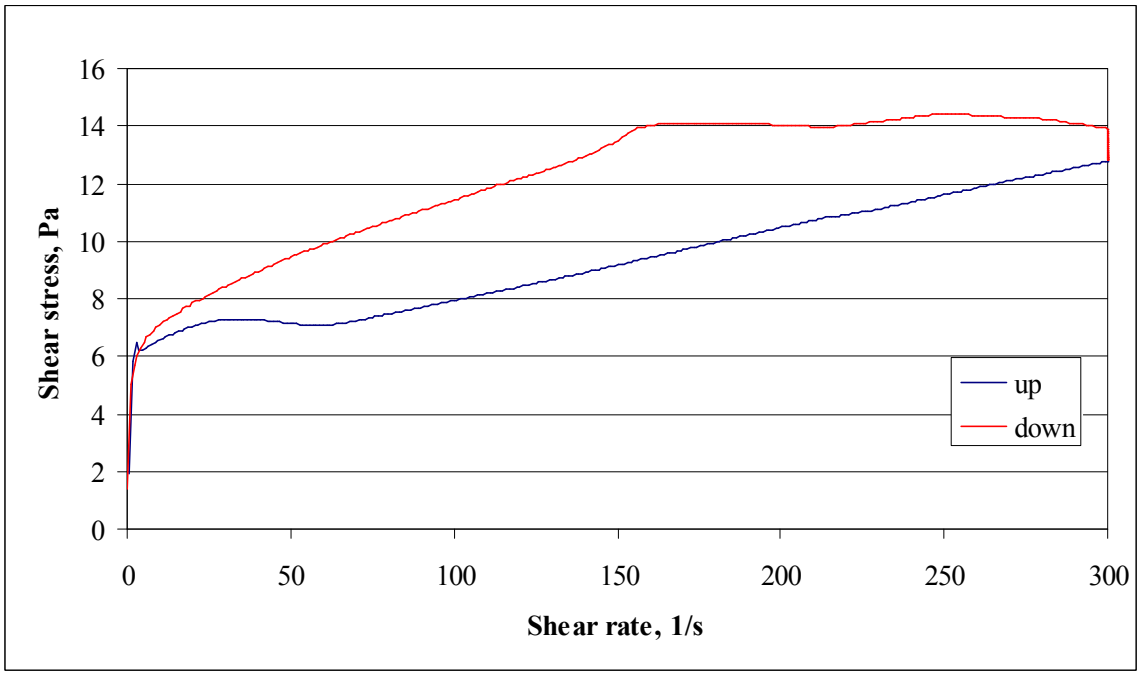

Figure 27 - SB7-2 SME Rheology Flow Curve

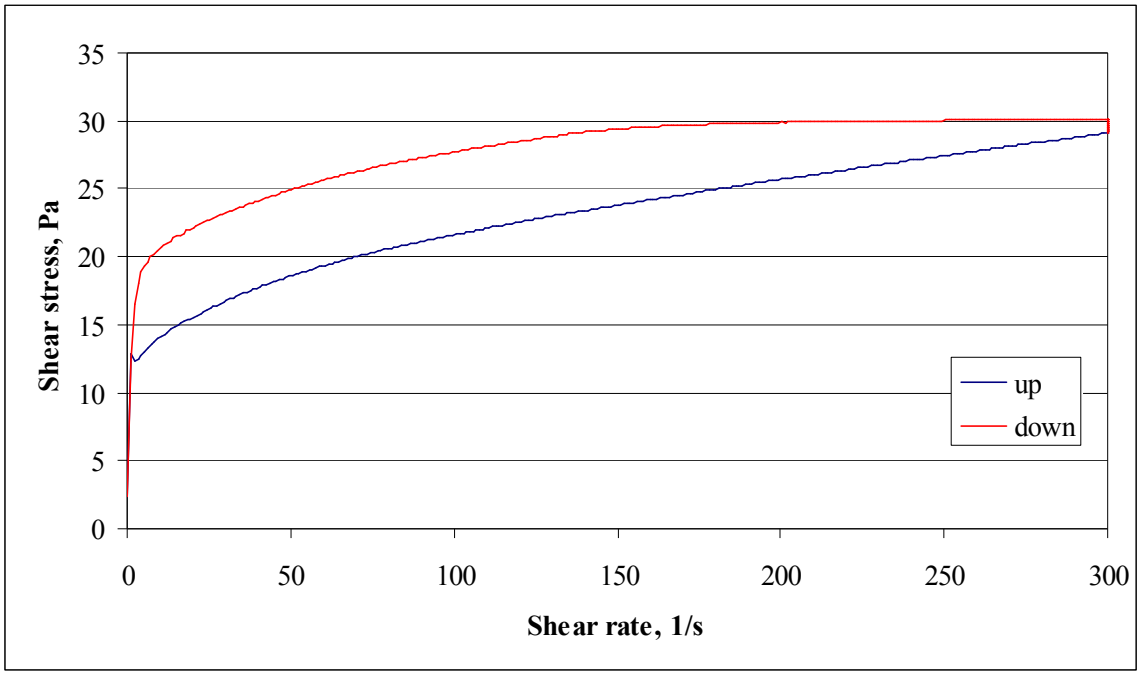

Figure 28 - SB7-3 SME Rheology Flow Curve

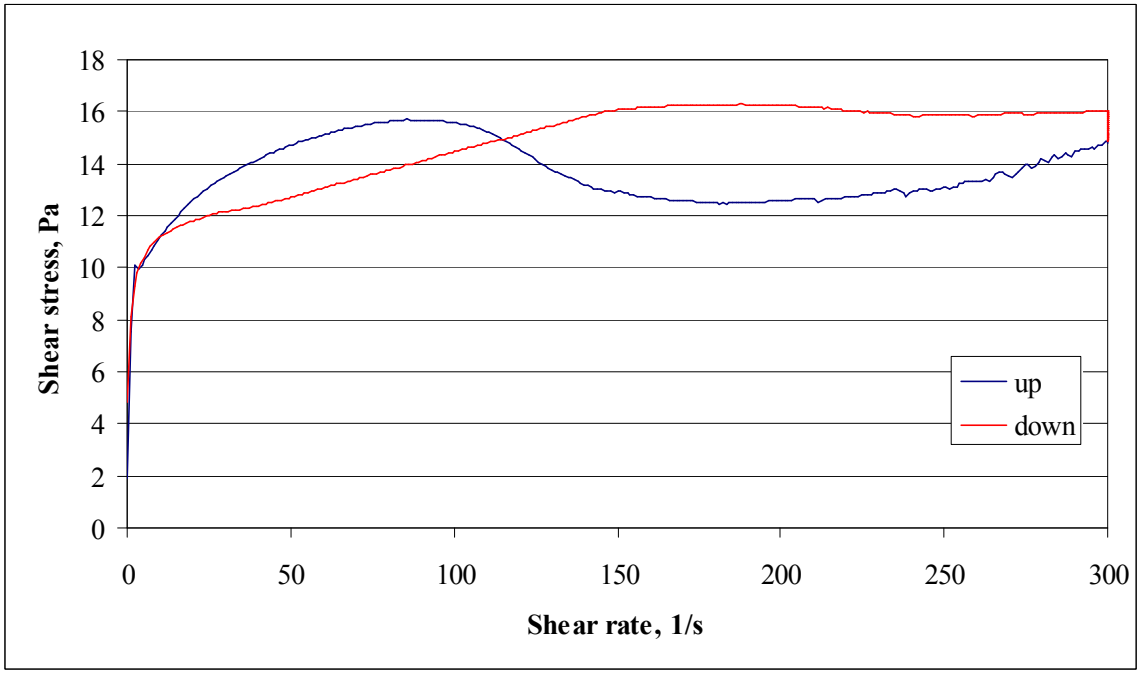

Figure 29 - SB7-4 SME Rheology Flow Curve

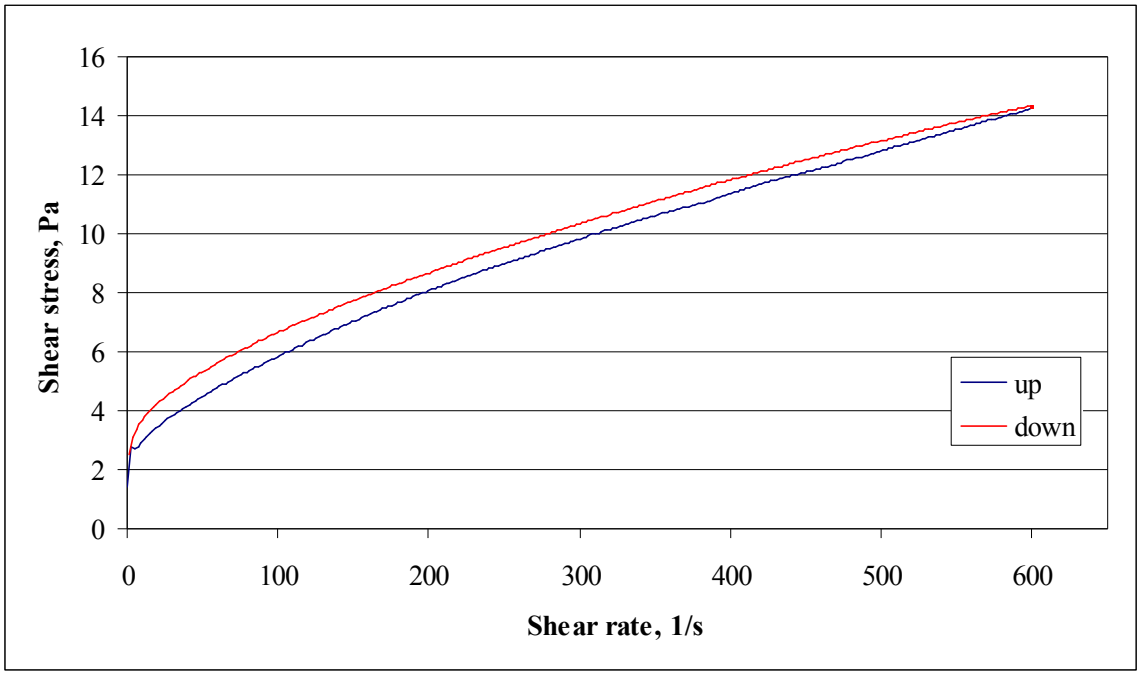

Figure 30 - SB7-5 SRAT Rheology Flow Curve

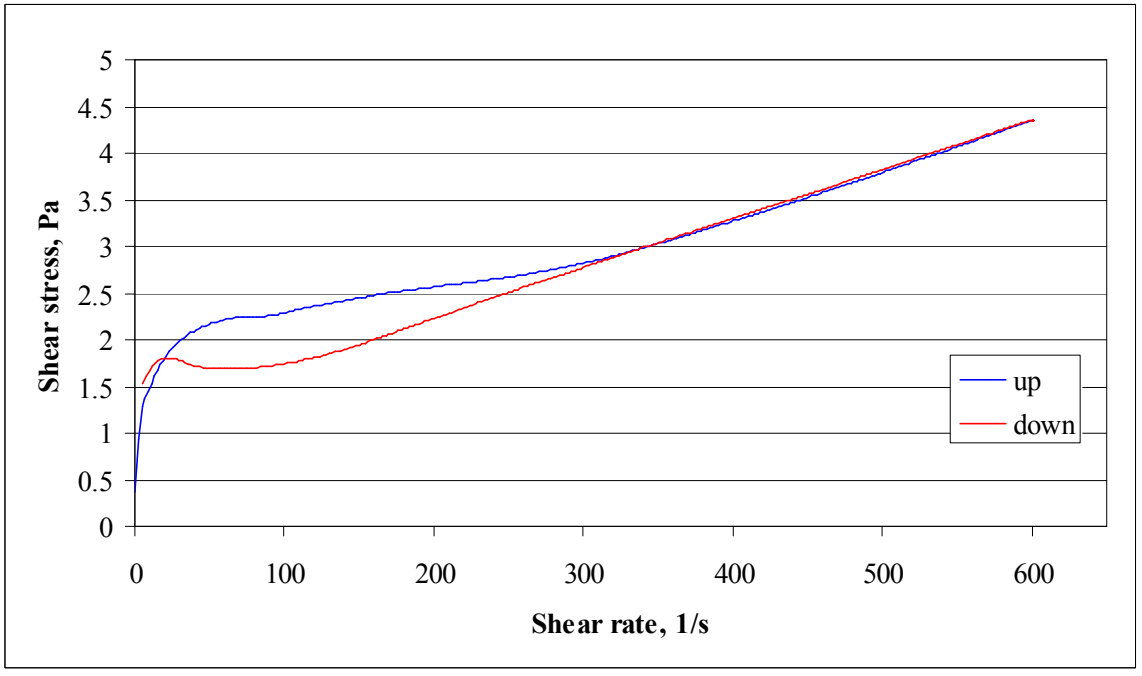

Figure 31 - SB7-6 SRAT Rheology Flow Curve

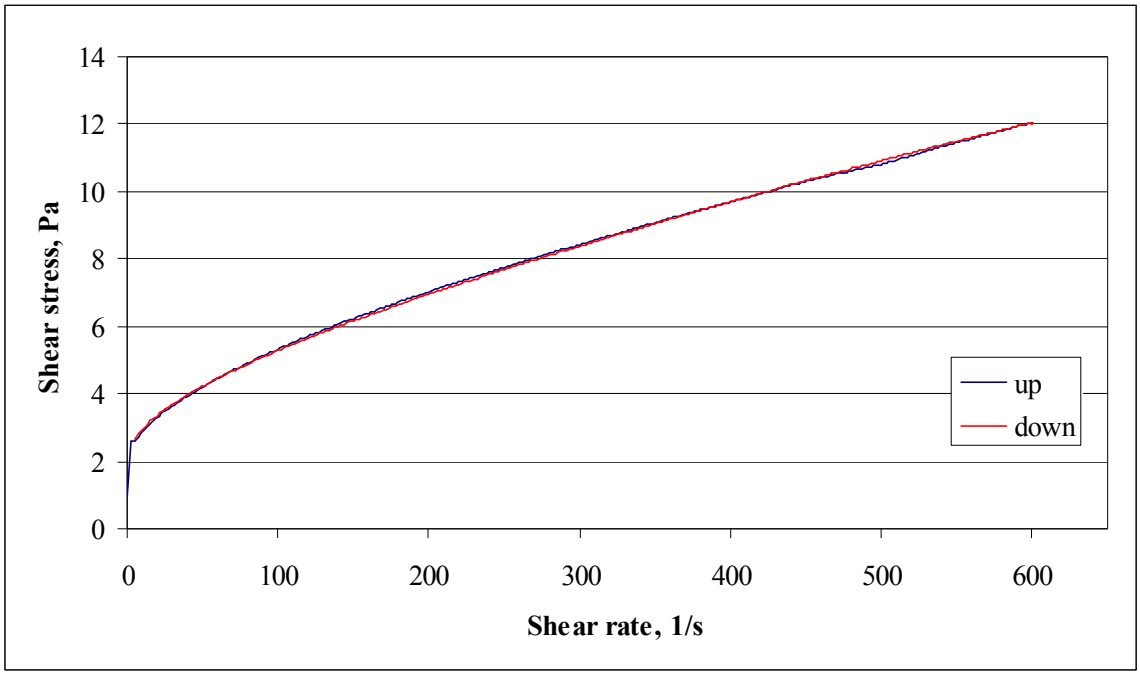

Figure 32 - SB7-7 SRAT Rheology Flow Curve

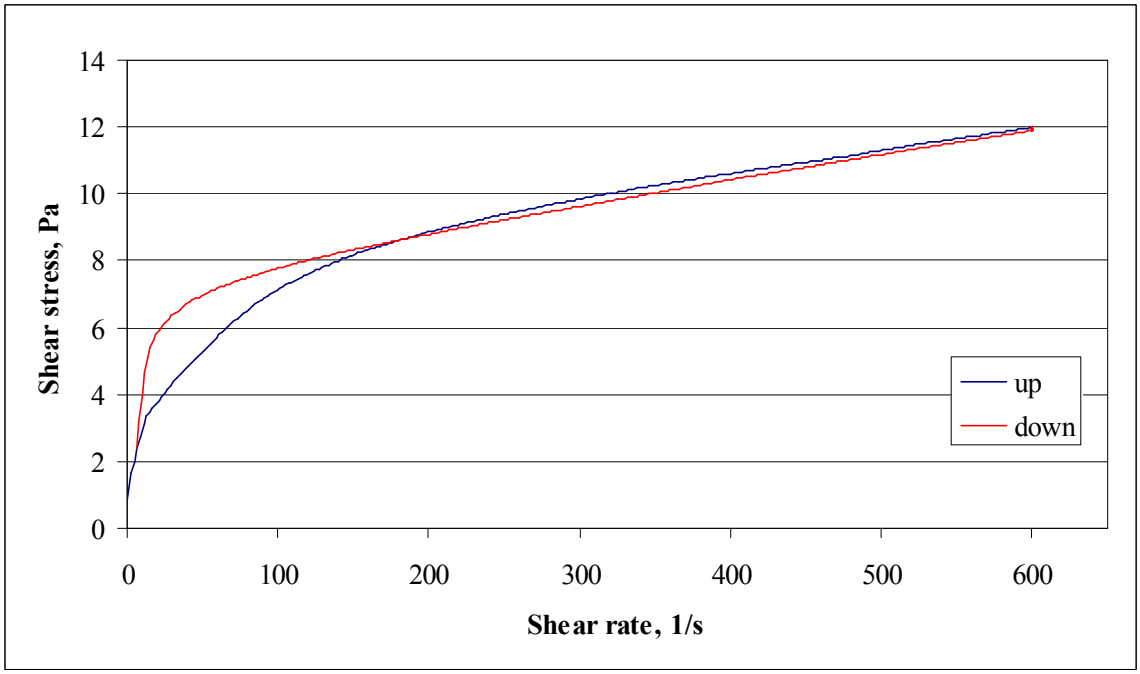

Figure 33 - SB7-8 SRAT Rheology Flow Curve

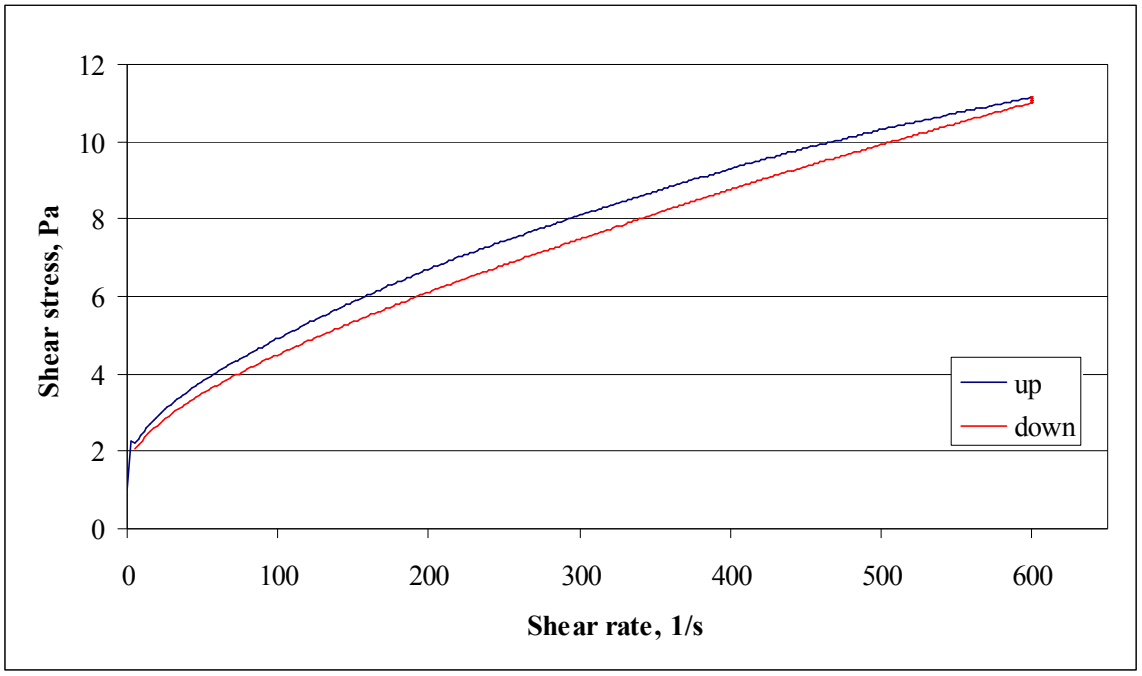

Figure 34 - SB7-9 SRAT Rheology Flow Curve

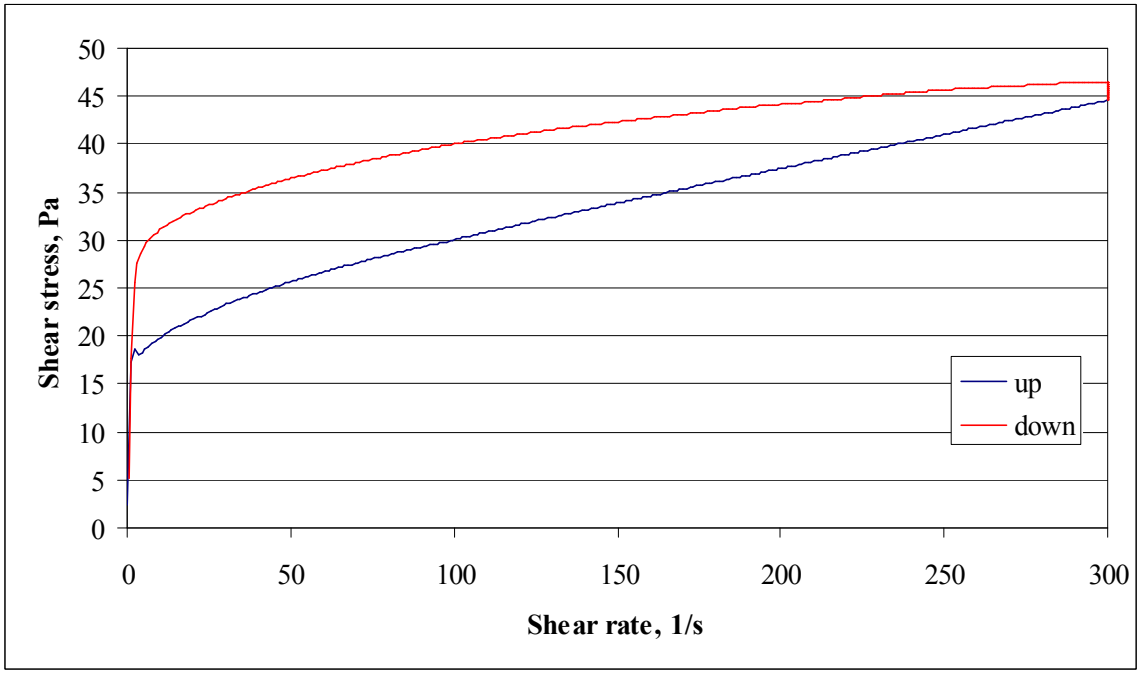

Figure 35 - SB7-5 SME Rheology Flow Curve

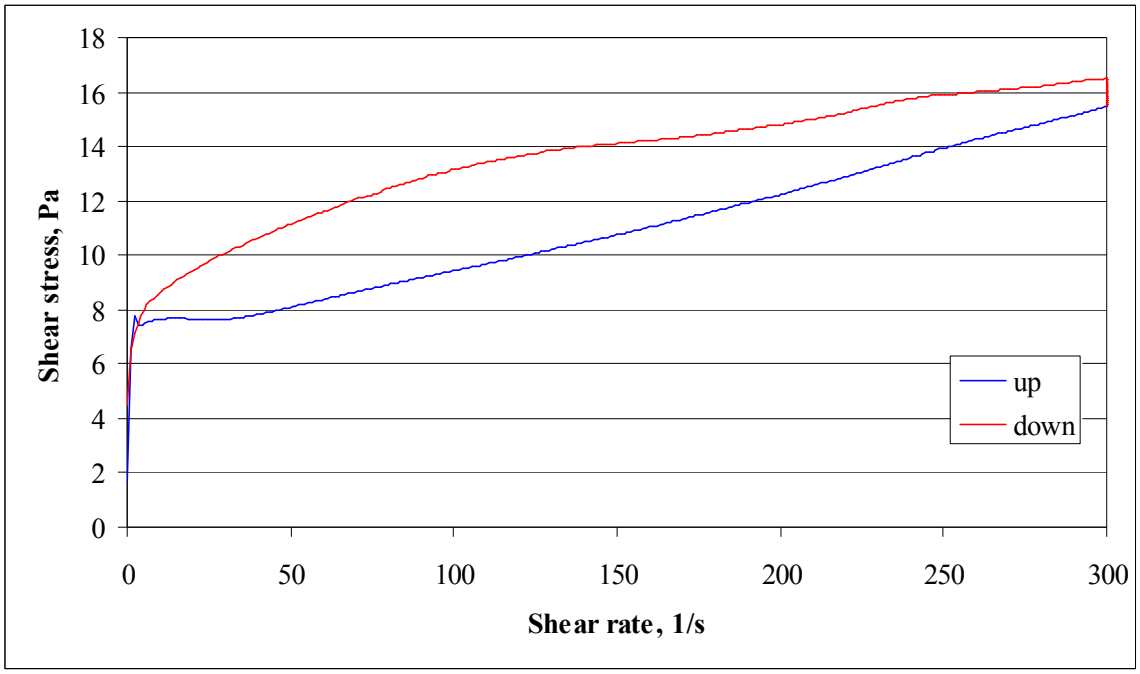

Figure 36 - SB7-6 SME Rheology Flow Curve

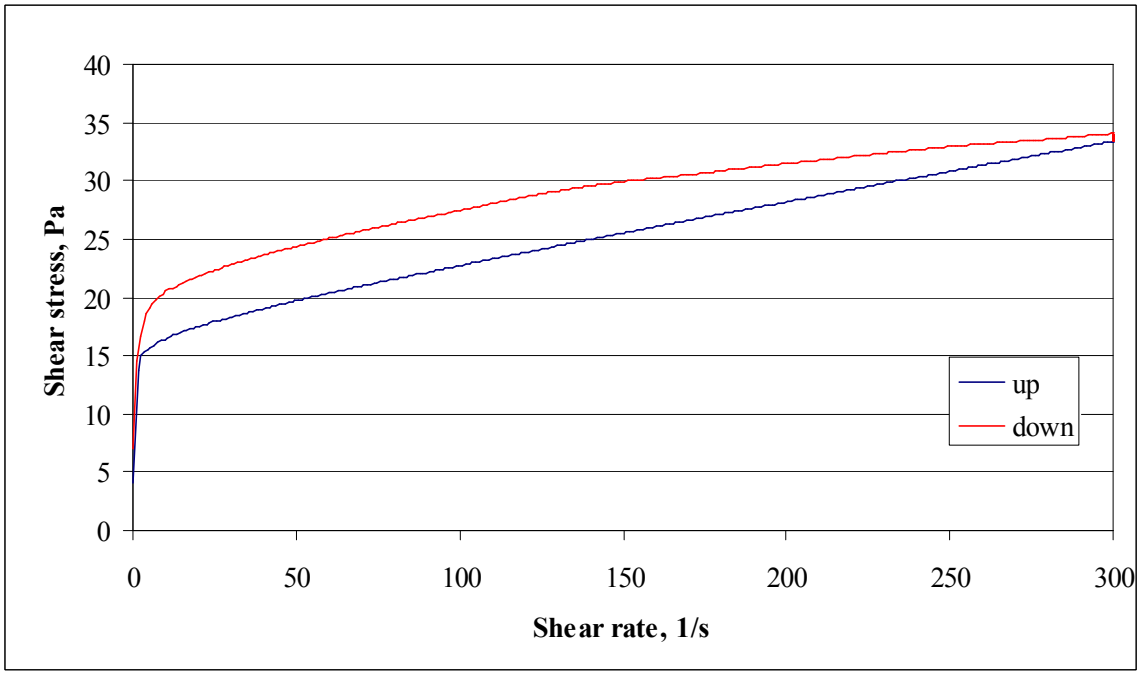

Figure 37 - SB7-7 SME Rheology Flow Curve

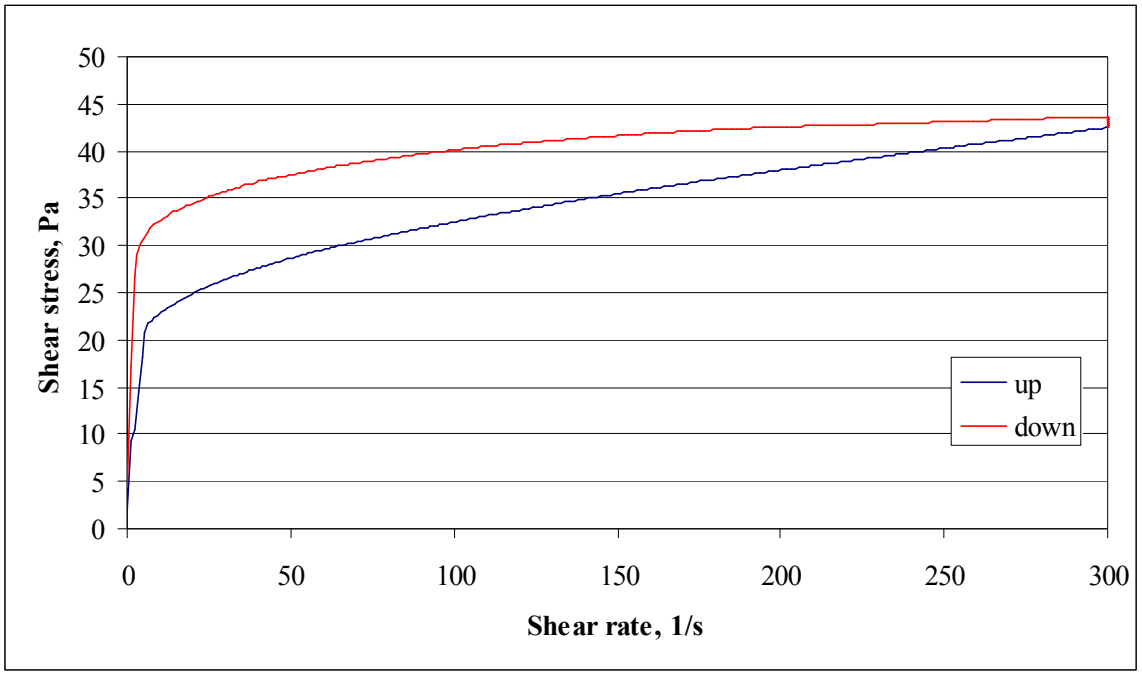

Figure 38 - SB7-8 SME Rheology Flow Curve

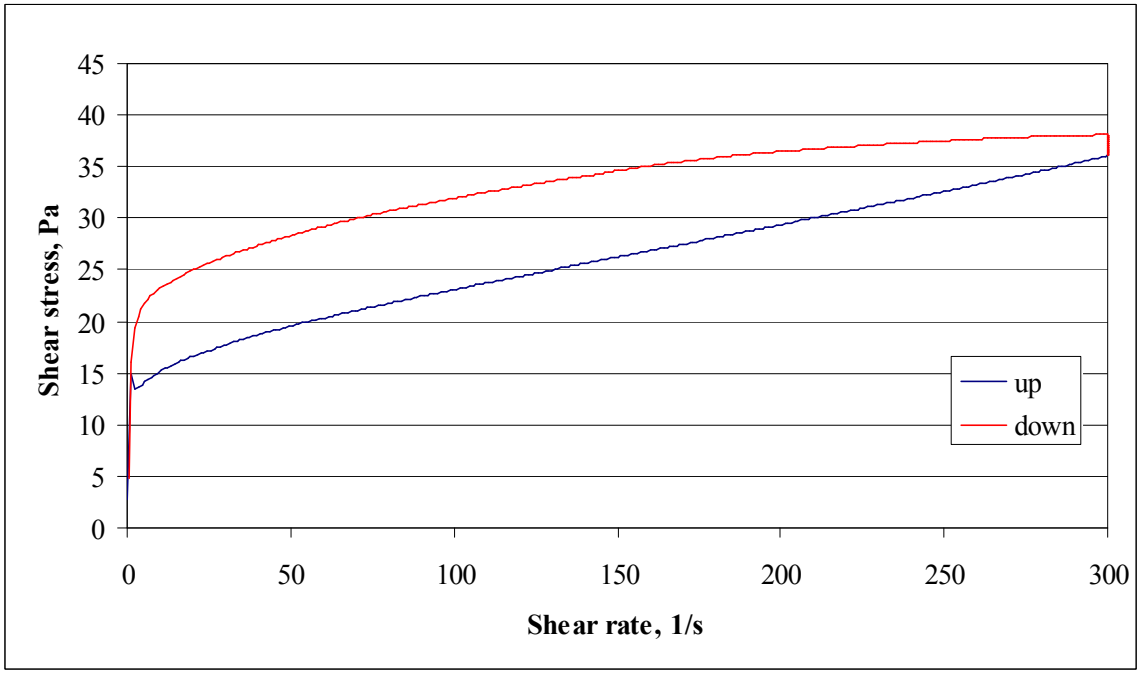

Figure 39 - SB7-9 SME Rheology Flow Curve

Distribution:

A. B. Barnes, 999-W
D. A. Crowley, 773-43A
S. D. Fink, 773-A
B. J. Giddings, 786-5A
C. C. Herman, 999-W
S. L. Marra, 773-A
P. R. Jackson, 773-A
A. S. Choi, 773-42A
J. M. Gillam, 766-H
B. A. Hamm, 766-H
J. F. Iaukea, 704-30S
D. C. Koopman, 999-W
D. P. Lambert, 999-W
J. D. Newell, 999-W
J. E. Occhipinti, 704-S
J. M. Pareizs, 773-A
D. K. Peeler, 999-W
J. W. Ray, 704-S
S. H. Reboul, 773-A
H. B. Shah, 766-H
D. C. Sherburne, 704-S
A.V. Staub, 704-27S
M. E. Stone, 999-W
J. R. Zamecnik, 999-W
J. M. Bricker, 704-27S
T. L. Fellinger, 704-26S
E. W. Holtzscheiter, 704-15S
M. T. Keefer, 766-H